DEFENSE DOCUMENTATION CENTER

FOR

SCIENTIFIC AND TECHNICAL INFORMATION

CAMERON STATION, ALEXANDRIA, VIRGINIA

A COMPARISON OF METHODS USED

FOR ANGULAR CORRELATION OF

ANNIHILATION RADIATION

BY SLIT GEOMETRY

W. E. Millett

(Supervising Professor)

R. N. Little

A COMPARISON OF METHODS USED

FOR ANGULAR CORRELATION OF

ANNIHILATION RADIATION

BY SLIT GEOMETRY

by

CHARLES JOSEPH VESELY, B.A., B.S.

THESIS

Presented to the Faculty of the Graduate School of

The University of Texas in Partial Fulfillment

of the Requirements

For the Degree of

Master of Arts

THE UNIVERSITY OF TEXAS

August 1963

PREFACE

The angular correlation of annihilation radiation by
slit geometry can be used to obtain the momentum distribu-
tion of annihilating electron-positron pairs in matter.
The purpose of this thesis is to describe, evaluate and
compare two types of apparatus employing rectangular slits
and two methods of data analysis that can be used in this
work.

The author wishes to express his gratitude to the
United States Air Force and the National Science Founda-
tion for their support in this work.

This research was suggested and directed by Dr. W. E.
Millett, to whom the author wishes to express his most
sincere appreciation.

The author is also indebted to his wife, Martha Kaye,
for her constant support and encouragement, to Mr. Louis
Deiterman for many stimulating discussions, and to the
staff of the Physics Shop, especially Mr. George Olewin,
who made possible the construction of the apparatus that
was finally decided upon.

<div align="right">C.J.V.</div>

June, 1963

<div align="center">3</div>

TABLE OF CONTENTS

CHAPTER I

DESCRIPTION OF THE TYPES OF APPARATUS

When a positron-electron pair annihilates by two
photon annihilation, the photons will be emitted in ex-
actly opposite directions if the pair is initially at
rest. A deviation of the angle between the emitted pho-
tons from 180° indicates an initial component of momen-
tum. This deviation from 180° has rarely been found to
exceed 15 milliradians. Angular correlation of these
photons over this range yields information about the
momentum distribution of the annihilating pairs.

The experimental configuration that employs rec-
tangular detectors is referred to as slit geometry.
Two types of apparatus employing slit geometry have
been used. One type[1,2] consists of two very long and
narrow slits with a single coincidence channel while
the other type[3,4] consists of eight narrow slits

[1] Berko, S., and Plaskett, J. S., Phys. Rev. 112,
1877 (1958).
[2] Berko, S., Phys. Rev. 128, 2166 (1962).
[3] Trumpy, G., Phys. Rev. 118, 668 (1960).
[4] Lovseth, J., "Positronium Formation and Dynamics
in Aluminum Oxide," Kjeller Research Establishment Re-
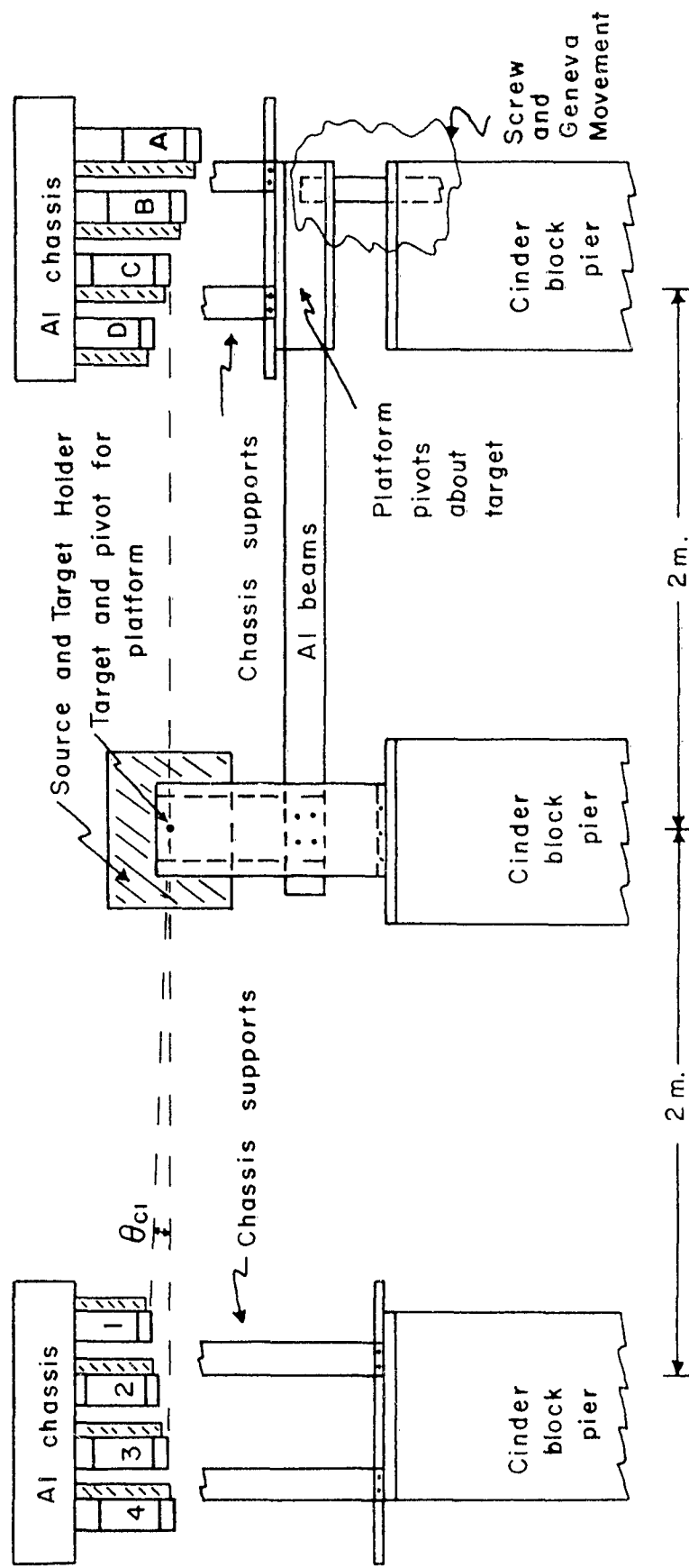port, Aug. 1962.

(four at each end) with sixteen coincidence channels. It was originally planned to construct a multiple coincidence channel apparatus here, but this plan was later changed because of the reasons that will be discussed in this thesis. Some work was done on this type of apparatus, however, and Figure 1 shows a sketch of the original plan modeled after Trumpy's[5] apparatus. This was later modified for single coincidence channel work, and a sketch of this apparatus is shown in Figure 2.

The major difference between the two instruments is the slit and photomultiplier tube arrangement. Instrument 1 (Figure 1) was to have used eight RCA 6342A photomultiplier tubes with a $1\frac{1}{2}$ inch diameter by $\frac{1}{4}$ inch thick NaI(Tl) crystal mounted directly on the photocathode of each. Four of these were to be mounted at each end of the instrument with lead shielding placed in such a way that only a lower slice of each crystal, the thickness of which would subtend an angle of 0.4 milliradian at the target, could detect radiation. The crystal slices at the stationary end were to have been 0.6 milliradian apart, and those at the movable end were to have been 2.4 milliradians apart making it possible to simultaneously measure 16 values of θ covering 9.6 milliradians in steps of 0.6 milliradian. Instrument 2 (Figure 2) uses two RCA 6342A photomultiplier tubes,

---

5
    Trumpy, G., op. cit.

Figure 1

Side View of 16 Coincidence

Channel Apparatus

(Not to Scale)

Stationary counters are numbered 1,2,3,4
Movable counters are numbered A,B,C,D.
Cross hatching indicates lead

Al chassis

A B C D

Source and Target Holder

Target and pivot for platform

Chassis supports

Al beams

Platform pivots about target

Screw and Geneva Movement

Cinder block pier

θ_{c1}

Chassis supports

Al chassis

1 2 3 4

Cinder block pier

Cinder block pier

2 m.

2 m.

SIDE VIEW OF 16 COINCIDENCE CHANNEL APPARATUS

Figure 2

Top View of Single Coincidence

Channel Apparatus

(Not to Scale)

Photo. tubes are marked A
Crystals are marked B
Cross hatcing indicates lead

Al platform

8"×.032" slit in lead

Al platform

A

B

Al beam

8"×.032" slit in lead

Al platform

Pivot

Target

Al beam

Source and Target Holder

Al beam

A

B

2 m.

2 m.

TOP VIEW OF SINGLE COINCIDENCE CHANNEL APPARATUS

each looking into the end of a 1 inch diameter by 8 inch long NaI(Tl) crystal. One tube and crystal are placed in lead shielding at each end of the instrument in such a manner that an 8 inch by .032 inch portion of the crystals is visible to the targets. The result is an instrument that employs one very long and very narrow slit at each end.
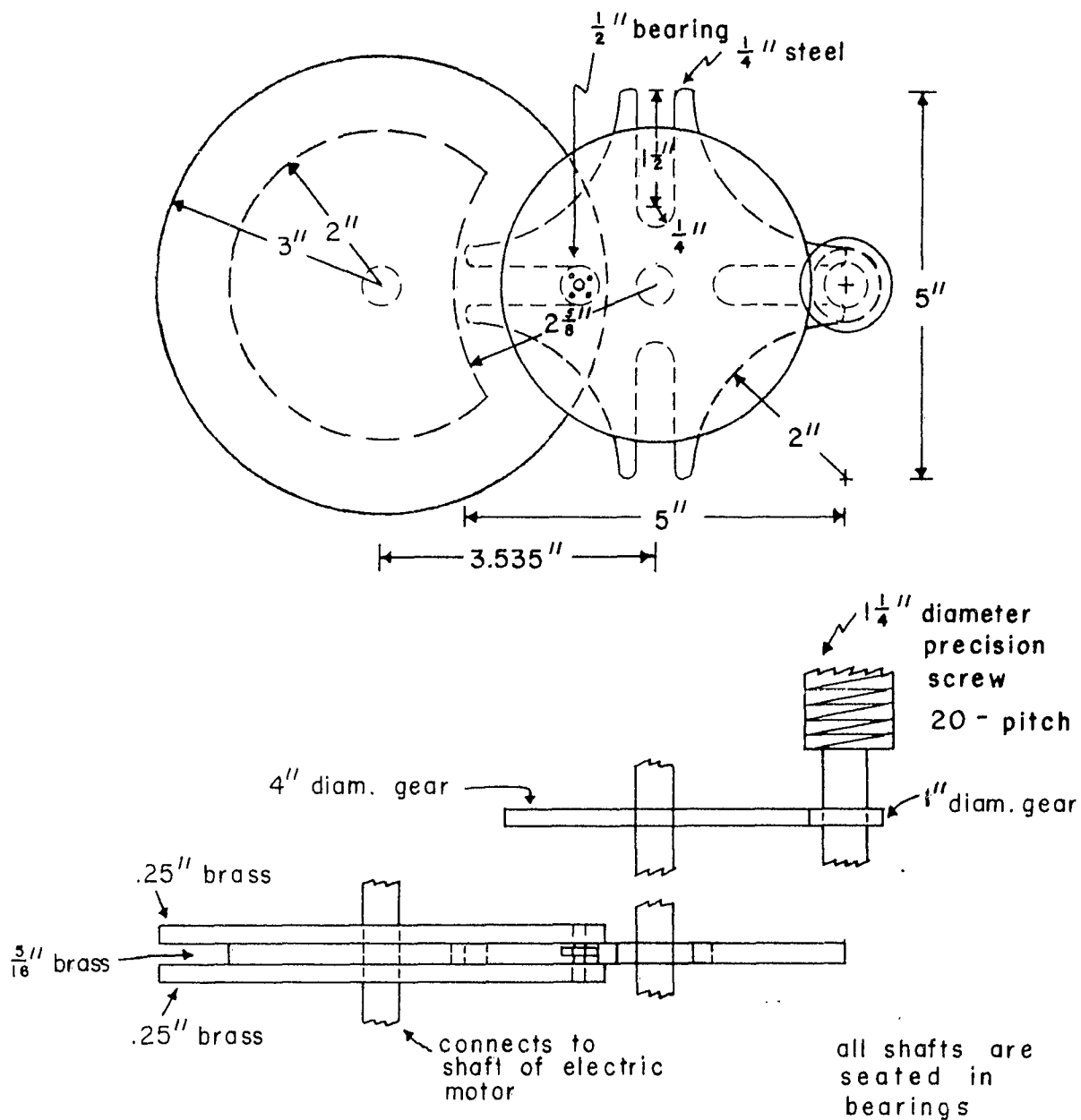
Three 32 inch high cinder block piers were constructed along a straight line 2 meters apart. The center pier supports the source and target holder, and the other two piers support the detectors. An 86 inch long platform made of aluminum was constructed so that one end pivots on a support at the central pier and the other end travels up and down on a precision screw mounted on one of the outer piers. The pitch of the screw is such that one full turn will increase or decrease the angle that the platform makes with the horizontal by 0.6 milliradian. The screw is linked to a four-pole Geneva Movement by one to four gear ratio so that one operation of the Geneva Movement will turn the screw through 360°. The Geneva Movement is powered by a reversible electric motor that can be programmed to turn the screw whenever a change in the angle between the slits is desired. A sketch of this mechanism is shown in Figure 3.

The source and target holder (see Figure 4) consists of a lead cylinder 10 inches in diameter by 10 inches long. Suitable means for adjusting the orientation of

Figure 3

Sketch of Screw and Geneva

Movement Mechanism

(Not to Scale)

$\frac{1}{2}''$ bearing $\frac{1}{4}''$ steel

$3''$ $2''$

$2\frac{3}{8}''$

$\frac{1}{2}''$

$\frac{1}{4}''$

$5''$

$5''$

$3.535''$

$2''$

$1\frac{1}{4}''$ diameter precision screw

20 - pitch

$4''$ diam. gear

$1''$ diam. gear

.25$''$ brass

$\frac{3}{16}''$ brass

.25$''$ brass

connects to shaft of electric motor

all shafts are seated in bearings

SKETCH OF SCREW AND GENEVA
MOVEMENT MECHANISM
(NOT TO SCALE)

Figure 4

Sketch of Source and Target Holder

(Not to Scale)

o-ring grooves are not shown

$3\frac{3}{4}''$

Sc₁

S

C

$\frac{S}{S}$

C

$\frac{S}{S}$

Ta

T

Sc₂

10''

$2\frac{1}{4}''$

Sc₁

S

S₁

$2\frac{7}{8}''$ C

5''

T

Sc₂

$3\frac{1}{4}''$
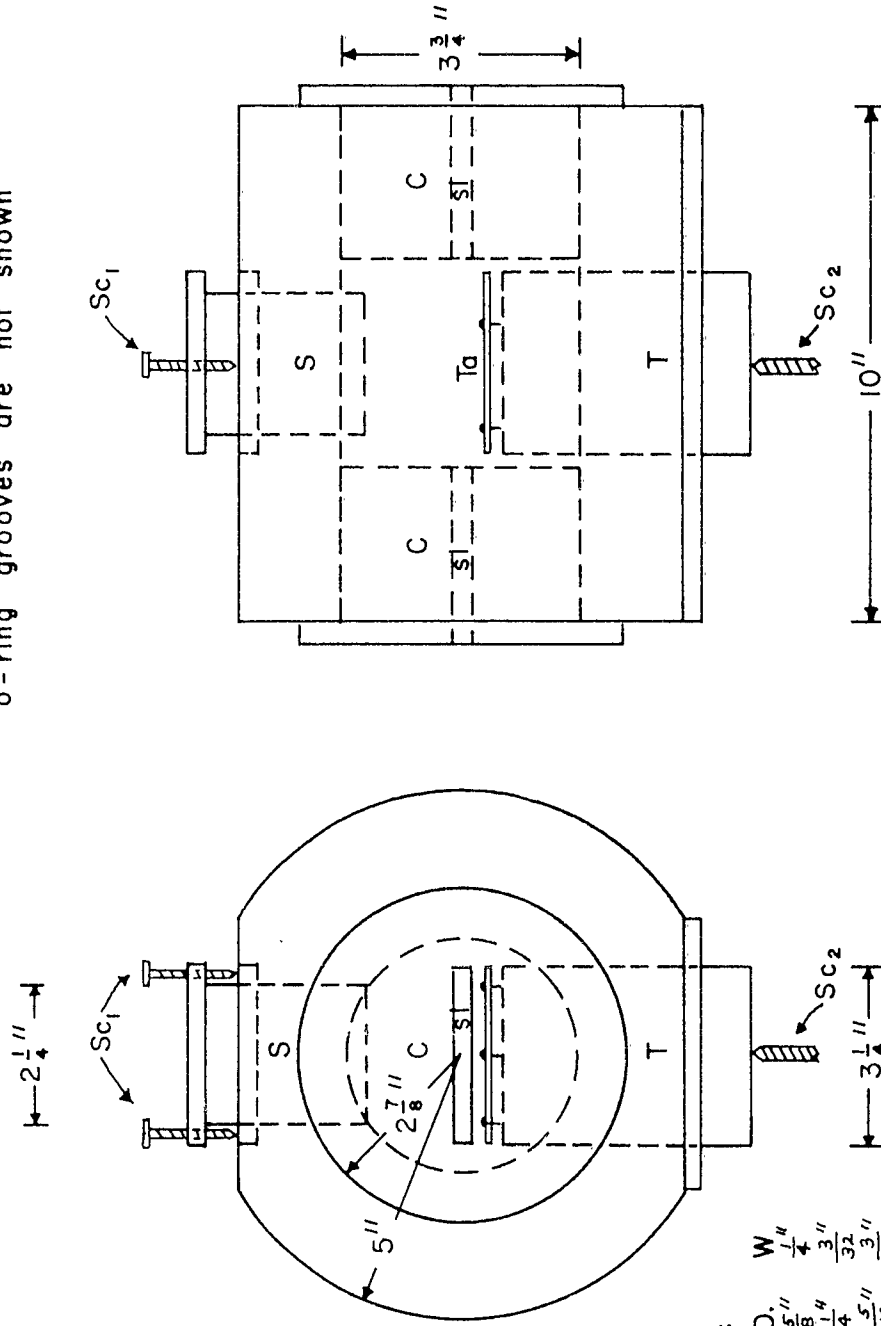
The following
size o-rings
are required:

O.D.	I.D.	W
$2 - 5\frac{1}{8}''$	$4\frac{5}{8}''$	$\frac{1}{4}''$
$1 - 3\frac{7}{16}''$	$3\frac{1}{4}''$	$\frac{3}{32}''$
$1 - 2\frac{1}{2}''$	$2\frac{5}{16}''$	$\frac{3}{32}''$
$1 - 2\frac{1}{4}''$	$2''$	$\frac{1}{8}''$
$1 - 3\frac{1}{4}''$	$3''$	$\frac{1}{8}''$

SOURCE AND TARGET HOLDER
(NOT TO SCALE)

the holder are provided so that its axis can be aligned with the axis of the instrument. The source is mounted on the end of a brass cylinder (S) that is inserted from the top. The depth of penetration is controlled by two brass screws (Sc_1). The target is mounted on a circular brass plate (Ta) that is connected to the face of a brass cylinder (T) by three equally spaced spring-loaded screws. This arrangement allows an orientation of the target that is independent of the orientation of the source and target holder. The target cylinder fits into the source and target holder from the bottom, and the brass cylinder rests upon a screw (Sc_2) that controls the depth of penetration. The collimators are two lead-filled brass cylinders (C) having rectangular slits (Sl) machined in the lead. These cylinders fit into each end of the source and target holder. O-ring grooves are provided wherever necessary so that the interior of the source and the target holder can be evacuated if later desired.

Solid state electronics is being used wherever possible. The output of each photomultiplier tube goes to a preamplifier and pulse shaper. The outputs from the pulse shapers go to the coincidence circuit, and the coincidence counts are scaled down by a factor of four. The output of the scale of four is then directed to the registers through a driver and switch. Schematics[6]
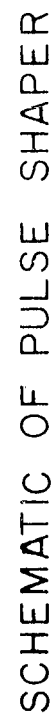
---

[6]
The development of the solid state electronics used in this apparatus was done by Mr. Louis Deiterman.

of the preamplifier, pulse shaper, and coincidence cir-
cuit are indicated in Figure 5, 6 and 7 respectively.
The original plan (16 coincidence channels) called for
a complex switch to direct the output of each coincidence
circuit to the correct sequence of registers. This switch
was designed and is shown in Figures 8 and 9 in case it
might be of future use.

Figure 5

Schematic of Preamplifier

SCHEMATIC OF PREAMPLIFIER

PM ANODE

Output

10 μf

.1 μf

1 μμf

1 μμf

1 μμf

Q1
Q2
Q3
Q5
Q6
Q7

SV5

-20
+20
-75

75 K
100K
220 K
15 K
4.7 K
150K
6.8 K
47 K
10 K
10 K
22 K
22 K
47 K
10K
3.3K
50 μf
.01 μf
10μf

Q1 2N317
Q2 2N315
Q3 2N248
Q5 2N315
Q6 2N248
Q7 2N315

Figure 6

Schematic of Pulse Shaper

SCHEMATIC OF PULSE SHAPER

Figure 7

Schematic of Coincidence Circuit

Switches are for counting singles

-6

Switch 2

4.7K

510 Ω

6.8K

2N711

Output

330 Ω

1000 μf

5K
Ri   1000 μμ
Input

Switch 1

15K

1K

IN916

IN29
39

5K

IK

Ri
1000 μμ

Input
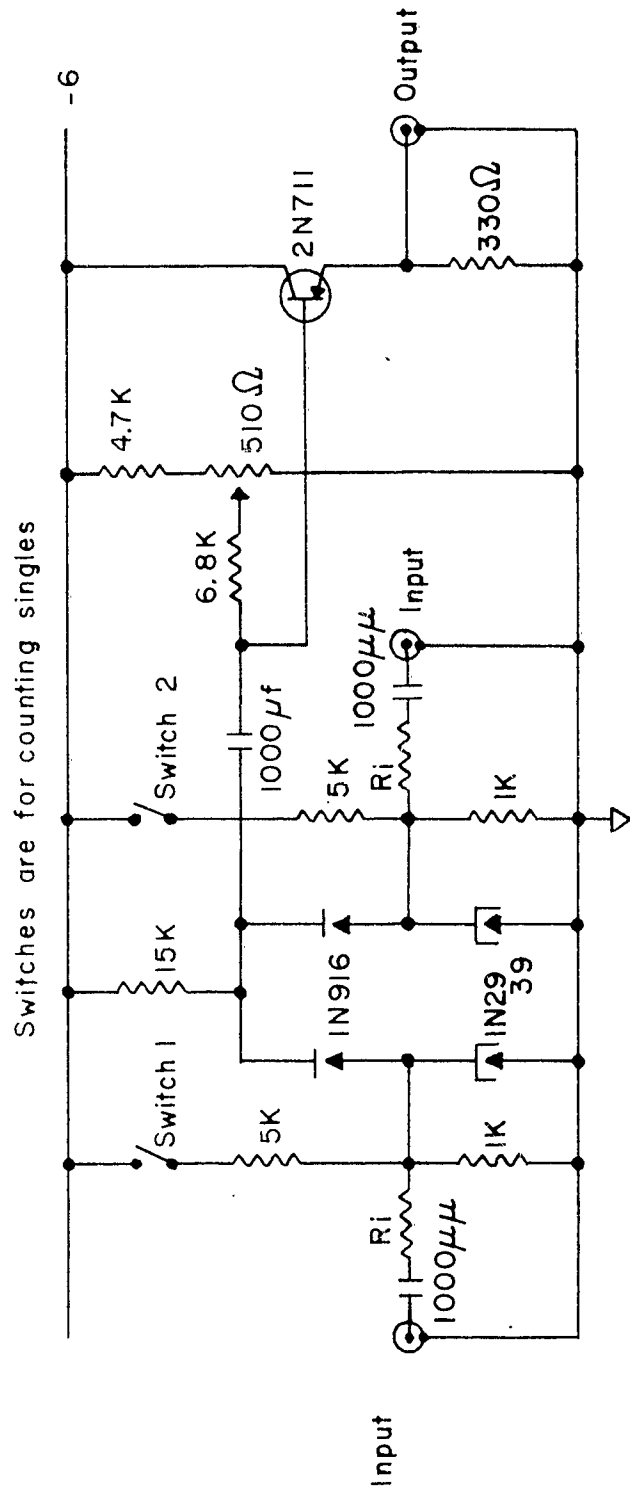
SCHEMATIC OF COINCIDENCE CIRCUIT

Figure 8

Schematic of Switch

(T-Bar Relays and Code)
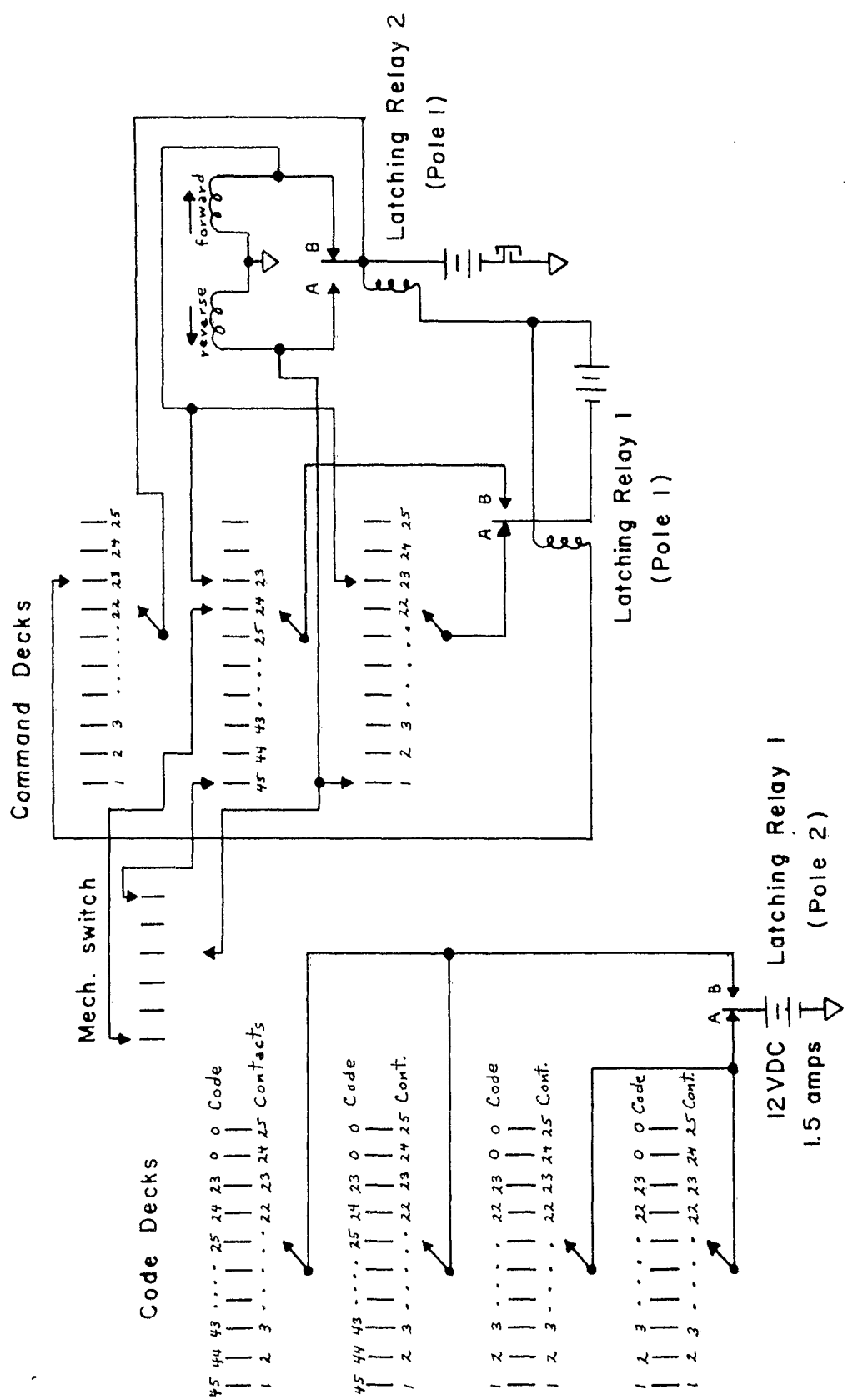
CONTROL SYSTEM FOR CODING THE RELAYS

Figure 9

Schematic of Switch

(Control System for Coding T-Bar Relays)

SCHEMATIC OF SWITCH

Coincidence Circuit	Relay A	Relay B	Relay C	Relay D	Relay E	Relay F	Register
A1	A1	B1	C1	D1	E1	F1	1
A2	A2 X B17	B2 X C9	C2 X D5	D2 X E3	E2 X F2	F2 X —	2
A3	A3 X B18	B3 X C10	C3 X D6	D3 X E4	E3 X F3	F3 X —	3
A4	A4 X B19	B4 X C11	C4 X D7	D4 X E5	E4 X F4	F4 X —	4
B1	A5 X B20	B5 X C12	C5 X D8	D5 X E6	E5 X F5	F5 X —	5
B2	A6 X B21	B6 X C13	C6 X D9	D6 X E7	E6 X F6	F6 X —	6
B3	A7 X B22	B7 X C14	C7 X D10	D7 X E8	E7 X F7	F7 X —	7
B4	A8 X B23	B8 X C15	C8 X D11	D8 X E9	E8 X F8	F8 X —	8
C1	A9 X B24	B9 X C16	C9 X D12	D9 X E10	E9 X F9	F9 X —	9
C2	A10 X B25	B10 X C17	C10 X D13	D10 X E11	E10 X F10	F10 X —	10
C3	A11 X B26	B11 X C18	C11 X D14	D11 X E12	E11 X F11	F11 X —	11
C4	A12 X B27	B12 X C19	C12 X D15	D12 X E13	E12 X F12	F12 X —	12
D1	A13 X B28	B13 X C20	C13 X D16	D13 X E14	E13 X F13	F13 X —	13
D2	A14 X B29	B14 X C21	C14 X D17	D14 X E15	E14 X F14	F14 X —	14
D3	A15 X B30	B15 X C22	C15 X D18	D15 X E16	E15 X F15	F15 X —	15
D4	A16 X —	B16 X C23	C16 X D19	D16 X E17	E16 X F16	F16 X —	16
	X —	B17 X C24	C17 X D20	D17 X E18	E17 X F17	F17 X 1	17
		B18 X C25	C18 X D21	D18 X E19	E18 X F18	F18 X 2	18
		B19 X C26	C19 X D22	D19 X E20	E19 X F19	F19 X 3	19
		B20 X C27	C20 X D23	D20 X E21	E20 X F20	F20 X 4	20
		B21 X C28	C21 X D24	D21 X E22	E21 X F21	F21 X 5	21
		B22 X C29	C22 X D25	D22 X E23	E22 X F22	F22 X 6	22
		B23 X C30	C23 X D26	D23 X E24	E23 X F23	F23 X 7	23
		B24 X —	C24 X D27	D24 X E25	E24 X F24	F24 X 8	24
		B25 X —	C25 X D28	D25 X E26	E25 X F25	F25 X 9	25
		B26 X —	C26 X D29	D26 X E27	E26 X F26	F26 X 10	26
		B27 X —	C27 X D30	D27 X E28	E27 X F27	F27 X 11	27
		B28 X —	C28 X —	D28 X E29	E28 X F28	F28 X 12	28
		B29 X —	C29 X —	D29 X E30	E29 X F29	F29 X 13	29
		B30 X —	C30 X —	D30 X —	E30 X F30	F30 X 14	30
		X —	X —	X —	X —	X 15	

CODE

Position	Relay A	Relay B	Relay C	Relay D	Relay E	Relay F
1	0	0	0	0	0	X
2	0	0	0	0	X	X
3	0	0	0	X	0	X
4	0	0	0	X	X	X
5	0	0	X	0	0	X
6	0	0	X	0	X	X
7	0	0	X	X	0	X
8	0	0	X	X	X	X
9	0	X	0	0	0	X
10	0	X	0	0	X	X
11	0	X	0	X	0	X
12	0	X	0	X	X	X
13	0	X	X	0	0	X
14	0	X	X	0	X	X
15	0	X	X	X	0	X
16	0	0	0	0	0	0
17	0	0	0	0	X	0
18	0	0	0	X	0	0
19	0	0	X	0	0	0
20	0	0	X	0	X	0
21	0	0	X	0	X	0
22	0	0	X	X	0	0
23	0	0	X	X	X	0
24	0	X	0	0	0	0
25	0	X	0	0	X	0
26	0	X	0	X	0	0
27	0	X	0	X	X	0
28	0	X	X	0	0	0
29	0	X	X	0	X	0
30	0	X	X	X	0	0
31	0	X	X	X	X	0
32	X	0	0	0	0	0
33	X	0	0	0	X	0
34	X	0	0	X	0	0
35	X	0	0	X	X	0
36	X	0	X	0	0	0
37	X	0	X	0	X	0
38	X	0	X	X	0	0
39	X	0	X	X	X	0
40	X	X	0	0	0	0
41	X	X	0	0	X	0
42	X	X	0	X	0	0
43	X	X	0	X	X	0
44	X	X	X	0	0	0
45	X	X	X	0	X	0

CHAPTER II

RESOLUTION AND DATA ANALYSIS

The momentum distribution of annihilation photons can be obtained from the data in two ways. The first method to be discussed (Method A) is to determine the resolution of the instrument in the z direction and from the data corrected in this manner to calculate the distribution in the z component of the momentum. The second method to be discussed (Method B) is to determine the θ resolution of the instrument (where $\pi - \theta$ is the angle between the photons) and from the data corrected in this manner to calculate the distribution in the ρ -component (where $p_\rho = \sqrt{p_x^2 + p_z^2}$) of the momentum. The results obtained from each method allow calculation of the total momentum distribution of annihilation photons.

The following discussion will refer to a coordinate system that is centered at the target with the z-axis vertical and the y-axis along the horizontal line defined by the source and the stationary slit.

A. Method A

This method has been used by several authors[7,8] and will be discussed in some detail. The finite resolution of the apparatus is a result of the finite dimensions of the target and of the slits. Since the z component of the momentum is being measured, it is desirable to have as narrow a resolution function in the z direction as possible. The calculation of the resolution function will show that this requirement makes it necessary to use a target and slits that are very narrow in the z direction. The stationary slit will be referred to as Slit A and the movable slit will be referred to as Slit B. Each slit has the dimensions of $2b_0$ in the z direction and $2a_0$ in the x direction and is a distance r_0 from the target.

If an annihilation pair at the origin have a momentum component in the z direction of p_z and if one photon passes along the y-axis through the center of Slit A (see Figure 10), the other photon must necessarily arrive at the plane of Slit B at a distance

$$z = \frac{p_z \, r_0}{m \, c} \tag{1}$$

from the x-y plane and a distance $r = \sqrt{x^2 + z^2}$ from the

---

[7] L. G. Lang, "Angular Correlation of Annihilation Radiation from Solids," Carnegie Institute of Technology Report, Sept. 1956.

[8] R. E. Green and A. T. Stewart, Phys. Rev, **98**, 486 (1955).
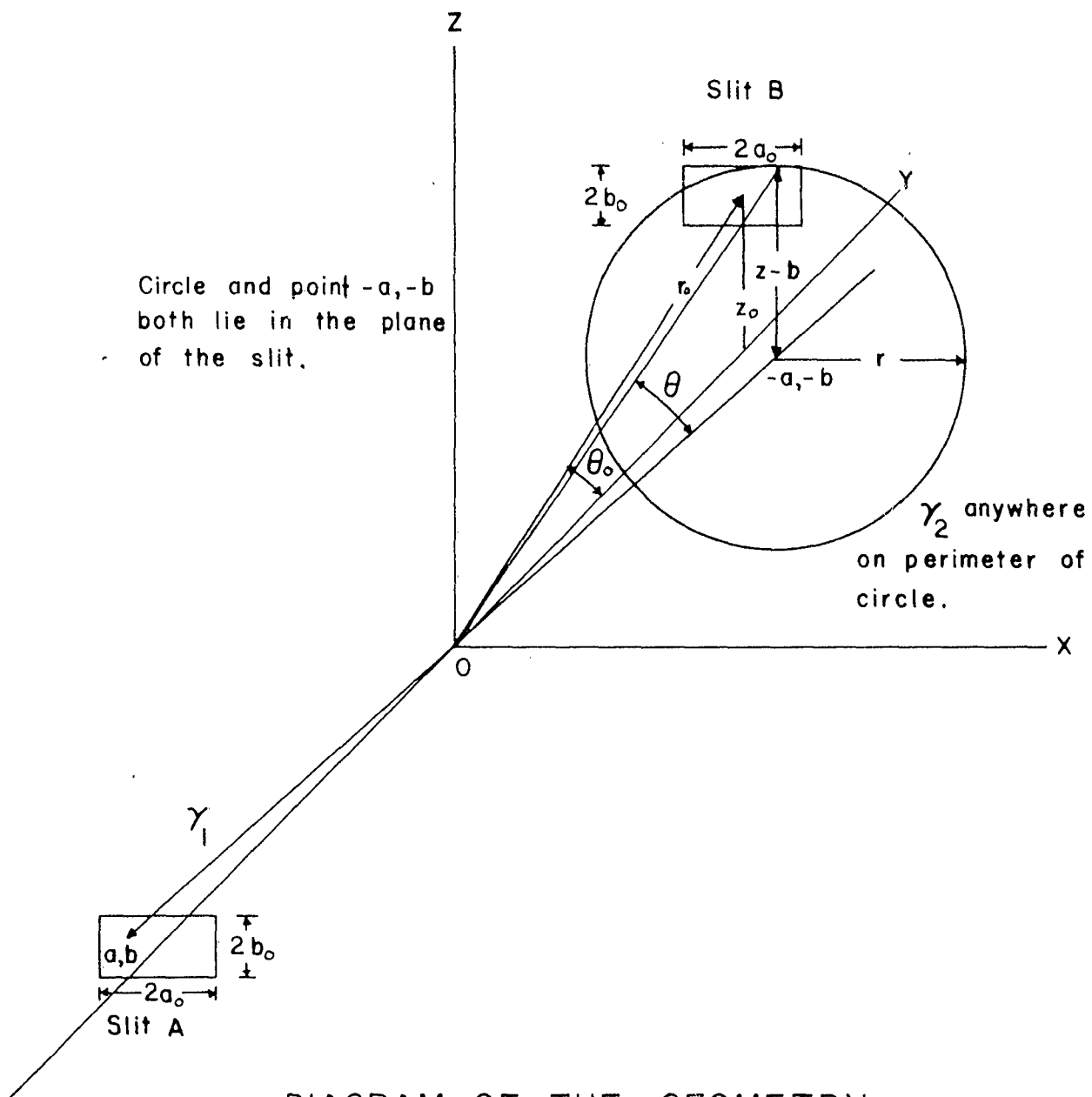
Figure 10

Diagram of the Geometry

DIAGRAM OF THE GEOMETRY

y-axis where z is a constant for a particular p_z and where

$$x = \frac{p_x r_0}{mc}$$

(2)

varies from $x = 0$ to $x = \frac{p_{x\,max}\,r_0}{mc}$.

If an annihilation pair at the origin have a momentum component in the z direction of p_z and if one photon passes through Slit A at the point a,b, the other photon must necessarily arrive at the plane of Slit B a distance of z-b above the x-y plane and a distance r from the y-axis where

$$r = \sqrt{(z-b)^2 + (x-a)^2}$$

(3)

and z is again a constant for a particular z. If Slit B is a set distance z_0 above the x-y plane, then a coincidence can only be detected if $z_0 - b_0 \leq z - b \leq z_0 + b_0$ and if $-a_0 \leq x - a \leq a_0$. This condition assumes constant efficiency of the scintillators in the x direction and in the z direction.

If the condition that $-a_0 \leq x - a \leq a_0$ is satisfied, coincidences will begin to occur for $z = z_0 - 2b_0$, will increase until $z = z_0$, and will decrease to zero at $z = z_0 + 2b_0$. Hence, the resolution curve for an annihilation at the origin will have a base width of 4bo centered about $z = z_0$. The increase is identical to the decrease because of the symmetry about z_0 and is linear, assuming constant efficiency of the scintillators in the

z direction. Therefore, the resolution function will be an isosceles triangle with a base width of $4b_0$ or twice the width of the slit in the z direction.

This resolution function can be generalized for a target of finite thickness in the following manner.[9] Consider a target having a width of 2t in the z direction. A single isosceles triangle of unit height centered at z_0 is given by

$$f(z_0, z) = \begin{cases} 1 - \dfrac{|z - z_0|}{2b_0} & , \quad |z - z_0| < 2b_0 \\ 0 & , \quad |z - z_0| > 2b_0 \end{cases} \qquad (4)$$

so

$$\frac{\partial f(z_0, z)}{\partial z_0} = \frac{1}{2b_0} \qquad (5)$$

$$df(z_0, z) = \frac{dz_0}{2b_0} \qquad (6)$$

Hence, the total resolution function is given by

$$R(z) = \int_{-t}^{t} f(z_0, z) \frac{dz_0}{2b_0} = \int_{-t}^{t} \left(1 - \frac{|z - z_0|}{2b_0} \right) \frac{dz_0}{2b_0} \qquad (7)$$

The function must be integrated in three parts.

$$R_I(z) = \int_{-t}^{z + 2b_0} \left[1 - \left(\frac{z_0}{2b_0} - \frac{z}{2b_0} \right) \right] \frac{dz_0}{2b_0} \quad ; \quad -t - 2b_0 \leq z \leq t - 2b_0$$

$$= \frac{1}{2} \left[\left(\frac{z}{2b_0} + 1 \right) + \frac{t}{2b_0} \right]^2 \qquad (8)$$

___

[9] This follows the derivation given by L. G. Lang.

$$R_{II}(z) = \int_{-t}^{t} \left[1 - \left(\frac{z_0}{2b_0} - \frac{z}{2b_0} \right) \right] \frac{dz_0}{2b_0} \quad ; \quad t - 2b_0 \leq z \leq -t$$

$$= \frac{t}{b_0} \left(1 + \frac{z}{2b_0} \right)$$

$$\text{(9)}$$

$$R_{III}(z) = \int_{-t}^{z} \left[1 - \left(\frac{z}{2b_0} - \frac{z_0}{2b_0} \right) \right] \frac{dz_0}{2b_0} + \int_{z}^{t} \left[1 - \left(\frac{z_0}{2b_0} - \frac{z}{2b_0} \right) \right] \frac{dz_0}{2b_0} \quad ; \quad -t \leq z \leq t$$

$$= \frac{t}{b_0} - \frac{t^2}{4b_0^2} - \frac{z^2}{4b_0^2}$$

$$\text{(10)}$$

The result of equations 8, 9 and 10 is plotted in Figure 11 for $t = 0.12$ milliradians and $b_0 = .2$ milliradians. Figure 11 gives the total resolution curve in the z direction for a target that is 0.24 milliradians wide and for slits that are 0.4 milliradians wide. The curve is almost Gaussian shaped and has a half-width at half-maximum of about 0.23 milliradians.

If the condition $-a_0 \leq x - a \leq a_0$ for a point target is not fulfilled, a correlation cannot be detected even though the photon pair has a p_z that lies within the proper range.

The resolution function in the x direction can be calculated in exactly the same manner as above. For a point target located at the origin, it will have a total base width of $4a_0$, assuming constant crystal efficiency in the x direction. It is, therefore, possible to detect a correlated photon pair having a p_z in the proper range if $p_x \leq \frac{2a_0 mc}{r_0}$. Extending the resolution function to a

Figure 11

Resolution Curve for Method A

RESOLUTION CURVE

$\theta_o = 0.6$ mr.

$R(\theta)$

θ (MR.)
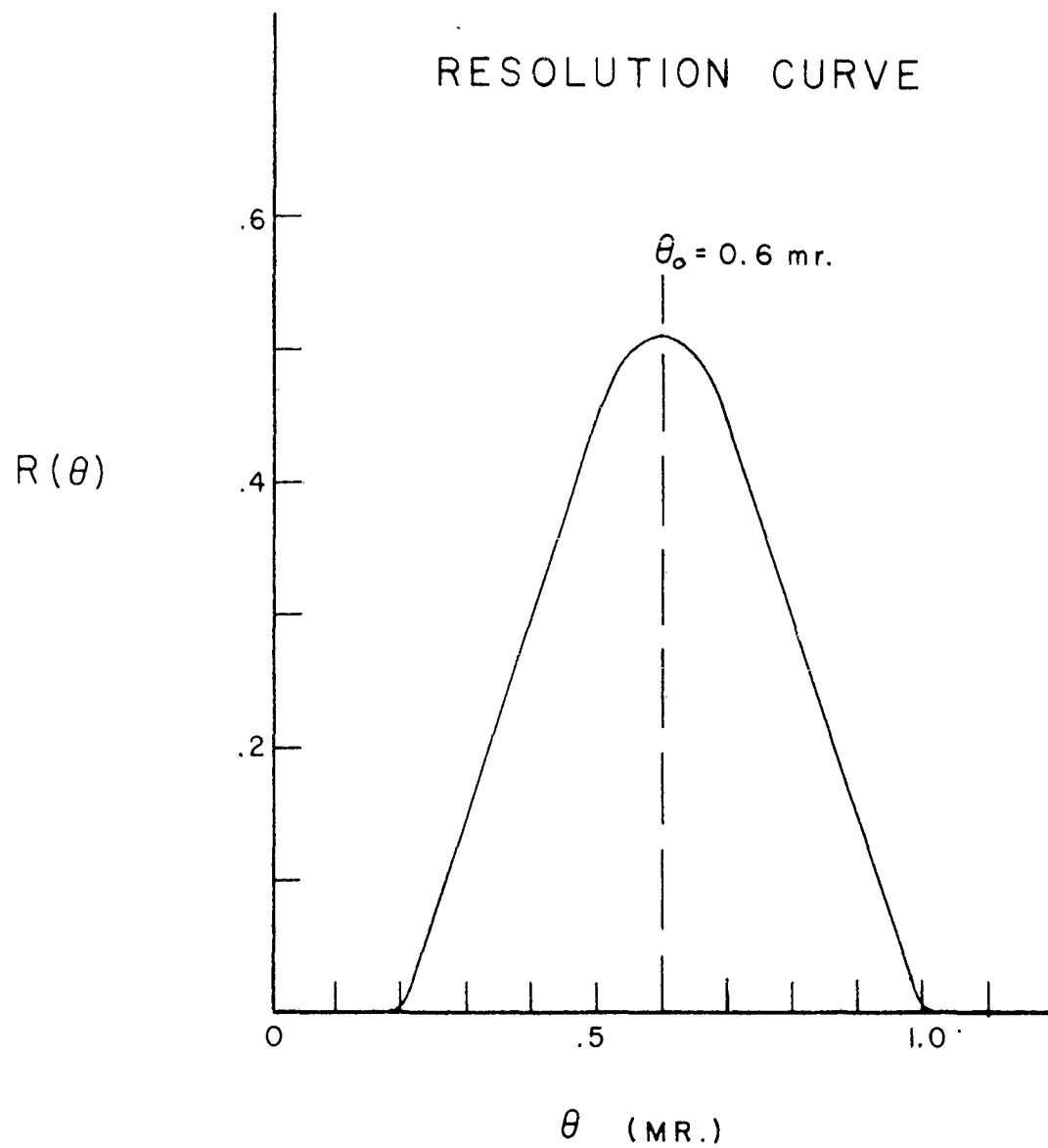
finite target in the same manner as above will give a base width even greater than $4a_0$.

If $2a_0 \gg \dfrac{p_{x\ max}\ r_0}{m\,c}$, it can be assumed that all photon pairs having a p_z in the proper range will be detected except when a is close to $\pm a_0$. If $2a_0$ is large enough, the correlations that are not counted because a is close to $\pm a_0$ can be neglected. Since $\dfrac{p_{x\ max}}{m\,c} \cong 10$ milliradians, the condition for making this approximation means that the slit length ($2a_0$) must be much greater than 10 milliradians.

The first step in the analysis of the data is to correct for the z direction finite resolution of the apparatus. This is done by employing the parabolic method of Eckart[10] at each of the data points. The effect of this correction is to increase the height of the peak and to sharpen the corners of the angular correlation curves.

When Slit B is displaced an amount z above the axis, the corrected coincidence counting rate $D(p_z)$ is proportional to the total number of pairs annihilating per unit time having $p_z = \dfrac{m\,c\,z}{r_0}$. When $2a_0 \gg \dfrac{p_{x\ max}\ r_0}{m\,c}$, the following relationship exists:

$$D(p_z) = const. \int_0^\infty \int_0^{2\pi} \rho(p)\, p_\rho\, dp_\rho\, d\phi \qquad (11)$$

10
    Eckart, C., Phys. Rev. 51, 735 (1937).

where $\rho(p)$ is the momentum space density of annihilating pairs and the integral is taken over the plane of constant p_z . It is assumed that variations in $\rho(p)$ are small within a region Δz corresponding to the slit width and that $\rho(p)$ is spherically symmetrical about the origin in momentum space. Now

$$p_\rho = \sqrt{p^2 - p_z^2} \tag{12}$$

so

$$dp_\rho = \frac{p\,dp}{\sqrt{p^2 - p_z^2}} \tag{13}$$

and a transformation of the variable p_ρ to p in the integral gives

$$D(p_z) = 2\pi\,const.\int_{p_z}^{\infty}\rho(p)\,p\,dp \tag{14}$$

since when $p_\rho = 0$, $p = p_z$ and when $p_\rho = \infty$, $p = \infty$.

Equation 14 can be differentiated with respect to p_z which gives

$$\frac{dD(p_z)}{dp_z} = -2\pi\,const.\,\rho(p_z)\,p_z \tag{15}$$

and solving for $\rho(p_z)$,

$$\rho(p_z) = -\frac{1}{2\pi\,const.\,p_z}\,\frac{dD(p_z)}{dp_z} \tag{16}$$

Now $p_z = \frac{mcz}{r_o}$, so

$$\rho(p_z) = -\frac{r_o^2}{2\pi m^2 c^2\,const.}\,\frac{dD(p_z)}{dz}\,\frac{1}{z} \tag{17}$$

Since $\rho(p)$ was assumed spherically symmetrical about the origin, $\rho(p_z) = \rho(p_x) = \rho(p_y) = \rho(p)$. Hence,

$$\rho(p) = - const. \frac{dD(p_z)}{dz} \frac{1}{z} \tag{18}$$

The momentum distribution $N(p)$ is given by

$$N(p) = 4\pi p^2 \rho(p) \tag{19}$$

where $4\pi p^2$ is the surface area of a sphere of radius p in momentum space. Substituting equation 18 into equation 19 gives the desired relation between corrected data and momentum distribution. The preceding derivation is due to Stewart.[11]

$$N(p) = - \frac{2}{const.} \frac{dD(p_z)}{dz} z \tag{20}$$

When the length of the slit $(2a_0)$ is not much greater than $\frac{p_{x\,max}\,r_0}{mc}$ then equation 20 does not hold for the relation between corrected data and momentum distribution. In this case, the corrected counting rate $D(p_z)$ is related to the total number of pairs annihilating per unit time having $p_z = \frac{mc\,z}{r_0}$ by the equation

$$D(p_z) = \int_{-a_o}^{a_o} \int_{-a_o+a}^{a_o-a} \int_{-\infty}^{\infty} \rho(p) p_\rho \, dp_y \, dp_x \, da \tag{21}$$

where a is the distance from the y-z plane that one of the photons of each detected annihilation pair entered Slit A. Without specific knowledge of the dependence of

---

11
   Stewart, A. T., op. cit.

$\rho(p)$ on p_x and p_y it is impossible to reduce equation 21 any further.

B. Method B

This method has been used by several authors[12,13,14] to analyze angular correlation data obtained by instruments employing cylindrical geometry but can also be used for slit geometry. The major problem is obtaining the resolution of the instrument as a function of θ and θ_0 where θ_0 is the correlation angle of the instrument and $\pi - \theta$ is the angle between annihilation photons.

Since θ and θ_0 will always be very small, the following approximations can be made. (See Figure 10)

$$y = r_0 \cos \theta_0 \cong r_0 \tag{22}$$

$$r = r_0 \sin \theta \cong r_0 \theta \tag{23}$$

$$z_0 = r_0 \sin \theta_0 \cong r_0 \theta_0 \tag{24}$$

If an annihilation pair at the origin have correlation angle θ and if one photon passes along the y-axis through the center of Slit A, the other photon must necessarily arrive at the plane of Slit B at a distance $r \cong r_0 \theta$

---

[12] Millett, W. E., and Castillo-Bahena, R., Phys. Rev. 108, 257, (1957).

[13] Castillo-Bahena, R., Ph.D. dissertation, The University of Texas, (1957) unpublished.

[14] Deiterman, L. H., Jr., M.A. thesis, The University of Texas, (1957) unpublished.

from the y-axis where

$$r = \sqrt{x^2 + z^2} = \frac{p_\rho \, r_0}{mc} = \frac{\sqrt{P_x^2 + P_z^2}}{mc} \, r_0 \, . \tag{25}$$

If Slit B is set at a distance z_0 above the x-y plane,

then a coincidence can be detected if $z_0 - b_0 \leq r \leq \sqrt{(z_0 + b_0)^2 + a_0^2}$.

If an annihilation pair at the origin have a correlation angle θ and if one photon passes through the opening of Slit A at the point a,b, the other photon must necessarily arrive at the plane of Slit B ($y \simeq r_0$) along the perimeter of a circle of radius $r \simeq r_0 \theta$ and with its center located at the point -a,-b. If Slit B is set at a distance z_0 above the x-y plane, then there is a chance for a coincidence being detected if some portion of the perimeter of the circle overlaps Slit B.

Assuming an isotropic momentum distribution, the probability that one photon of an annihilation pair located at the origin and having correlation angle θ will go through the area $\Delta a \, \Delta b$ at the point a,b in Slit A will be

$$P(A) = \frac{\Delta a \, \Delta b}{4 \pi r_0^2} \tag{26}$$

Let the probability that if one photon of an annihilation pair located at the origin and having correlation angle θ goes through the area $\Delta a \, \Delta b$ at the point a,b in Slit A, the other will pass through Slit B when it is set at an angle θ_0 be called P(B). Then the resolution function R(θ, θ_0) of the instrument for a point target

located at the origin when Slit B is set at an angle θ_0 will be given by

$$R(\theta, \theta_0) = \frac{1}{2\pi r_0^2} \int_0^{a_0} \int_{-b_0}^{b_0} P(B) \, da \, db \tag{27}$$

$P(B)$ will depend on θ_0, θ, and the point a,b, at which one of the photons of an annihilation pair enters Slit A.[15] It will be assumed that for each particular θ, θ_0, a,b that $P(B)$ is equal to the ratio of the arc of the circle whose radius is $r \simeq r_0 \theta$ that overlaps Slit B to the total perimeter of the circle.

There are nine different ways in which the arc of the circle can overlap the slit depending on the values of θ, θ_0, a, b, and the dimensions of the slit. These nine cases and the calculation of $P(B)$ for each are shown in Figures 12-20.

---

[15] This is only true when the annihilation takes place at the origin where the coordinates are 0,0.

Figure 12

$P(B)_A$ = No Arc Falls Within Slit B

$$P(B)_A$$

B

2 b_0

r

a,b

Proj. A

z_0

2 b_0

0,0

a_0
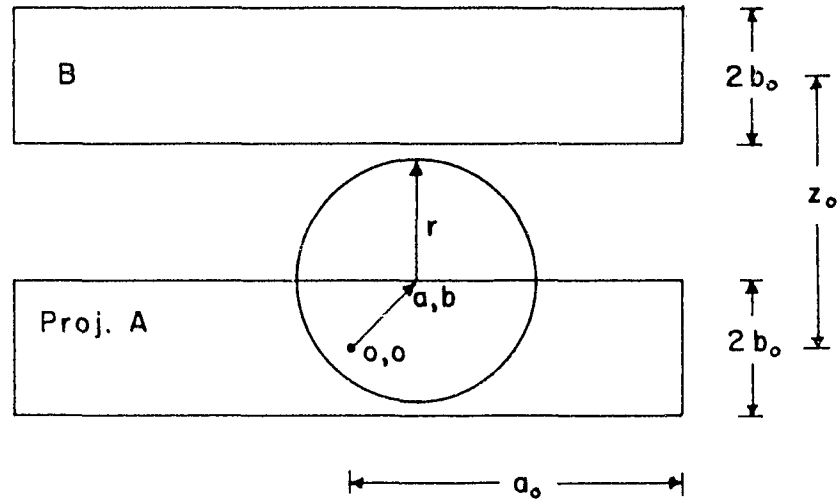
Proj. A means slit A projected onto plane of slit B.

$$P(B)_A = \frac{0}{2 \pi r} = 0$$

Figure 13

$P(B)_B$ - Arc Intersects Slit B

Twice on Lower Edge

$P(B)_B$
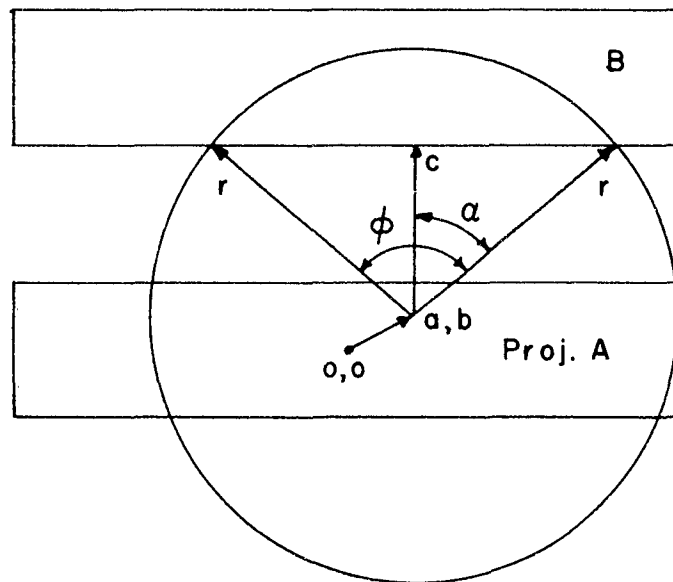
$$\alpha = \cos^{-1}\left(\frac{c}{r}\right) \qquad , \qquad c = z_0 - b_0 - b$$
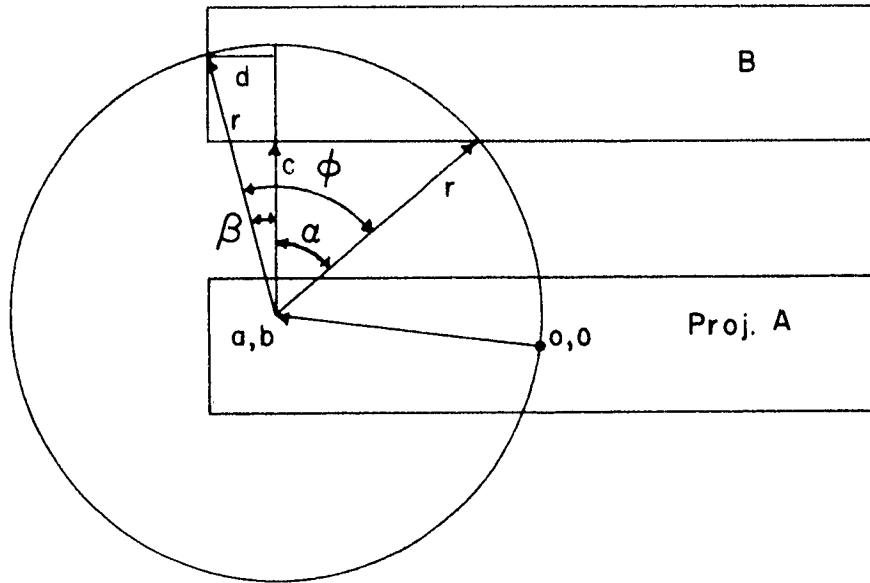
$$\phi = 2\alpha$$

$$P(B)_B = \frac{\phi r}{2\pi r}$$

$$P(B)_B = \frac{1}{\pi}\cos^{-1}\left(\frac{z_0 - b_0 - b}{r}\right)$$

Figure 14

$P(B)_C$ - Arc Intersects Slit B

Once on Lower Edge and

Once on Side

$$\alpha = \cos^{-1}\left(\frac{c}{r}\right) \quad , \quad c = z_0 - b_0 - b$$

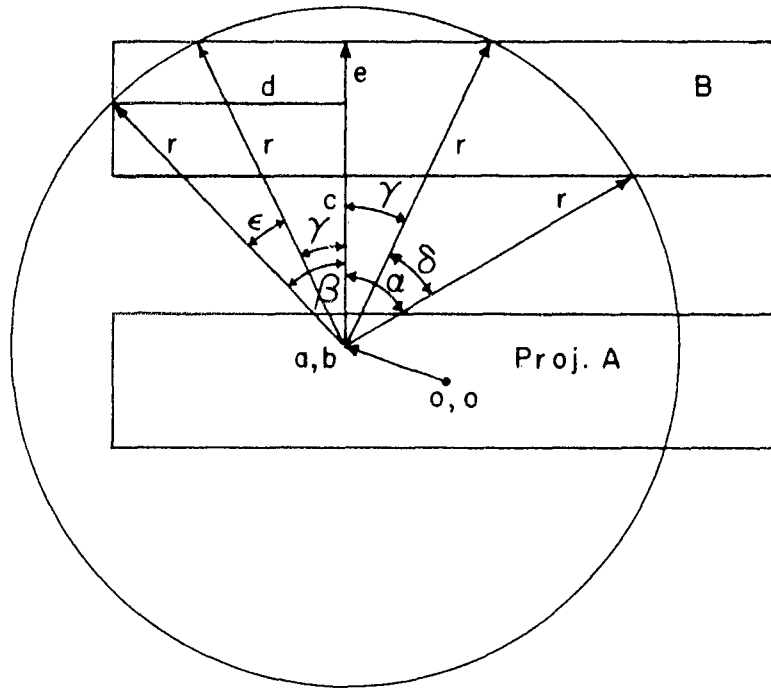$$\beta = \sin^{-1}\left(\frac{d}{r}\right) \quad , \quad d = a_0 - a$$

$$\phi = \alpha + \beta$$

$$P(B)_C = \frac{\phi r}{2\pi r}$$

$$P(B)_C = \frac{1}{2\pi}\left[\cos^{-1}\left(\frac{z_0 - b_0 - b}{r}\right) + \sin^{-1}\left(\frac{a_0 - a}{r}\right)\right]$$

Figure 15

$P(B)_D$ - Arc Intersects Slit B

Twice on Lower Edge and

Twice on Upper Edge

$$P(B)_D$$
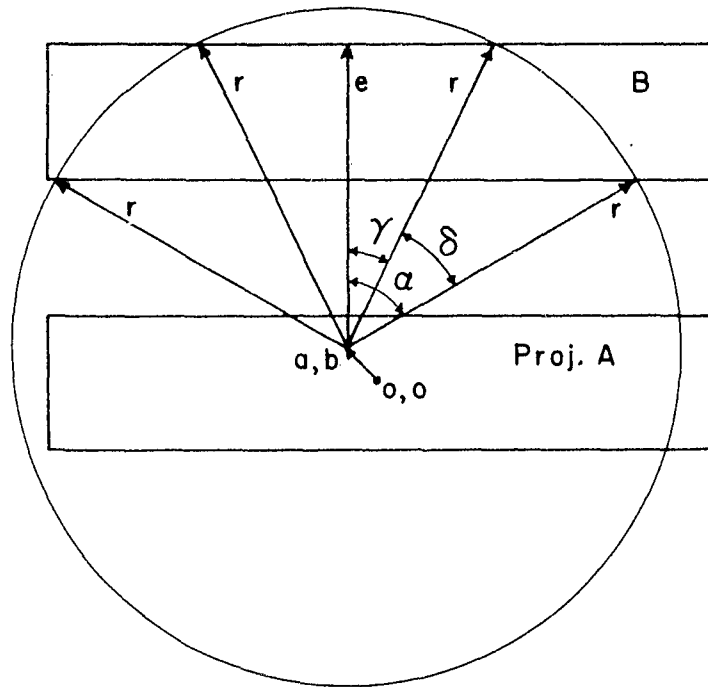
$$\alpha = \cos^{-1}\left(\frac{c}{r}\right) \qquad , \qquad c = z_o - b_o - b$$

$$\gamma = \cos^{-1}\left(\frac{e}{r}\right) \qquad , \qquad e = z_o + b_o - b$$

$$\delta = \alpha - \gamma \quad , \qquad \phi = 2\delta$$

$$P(B)_D = \frac{\phi r}{2\pi r}$$

$$P(B)_D = \frac{1}{\pi}\left[\cos^{-1}\left(\frac{z_o - b_o - b}{r}\right) - \cos^{-1}\left(\frac{z_o + b_o - b}{r}\right)\right]$$

Figure 16

$P(B)_E$ - Arc Intersects Slit B

Twice on Upper Edge,

Once on Lower Edge and

Once on Side

$$P(B)_E$$

$$\alpha = \cos^{-1}\left(\frac{c}{r}\right) \qquad , \qquad c = z_o - b_o - b$$

$$\gamma = \cos^{-1}\left(\frac{e}{r}\right) \qquad , \qquad e = z_o + b_o - b$$

$$\beta = \sin^{-1}\left(\frac{d}{r}\right) \qquad , \qquad d = a_o - a$$

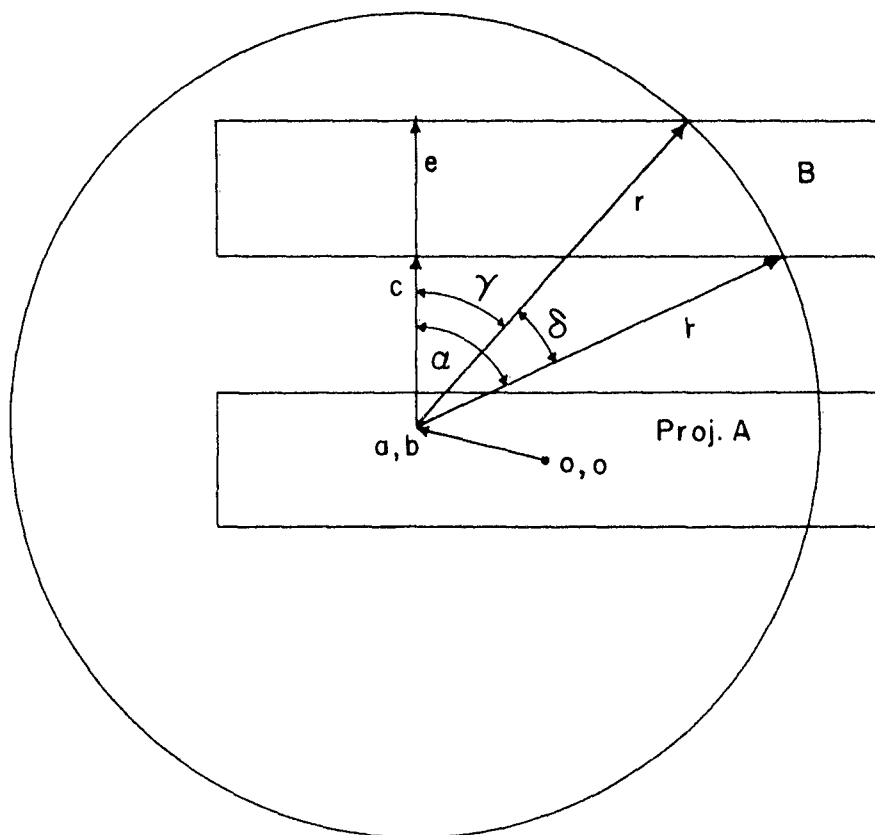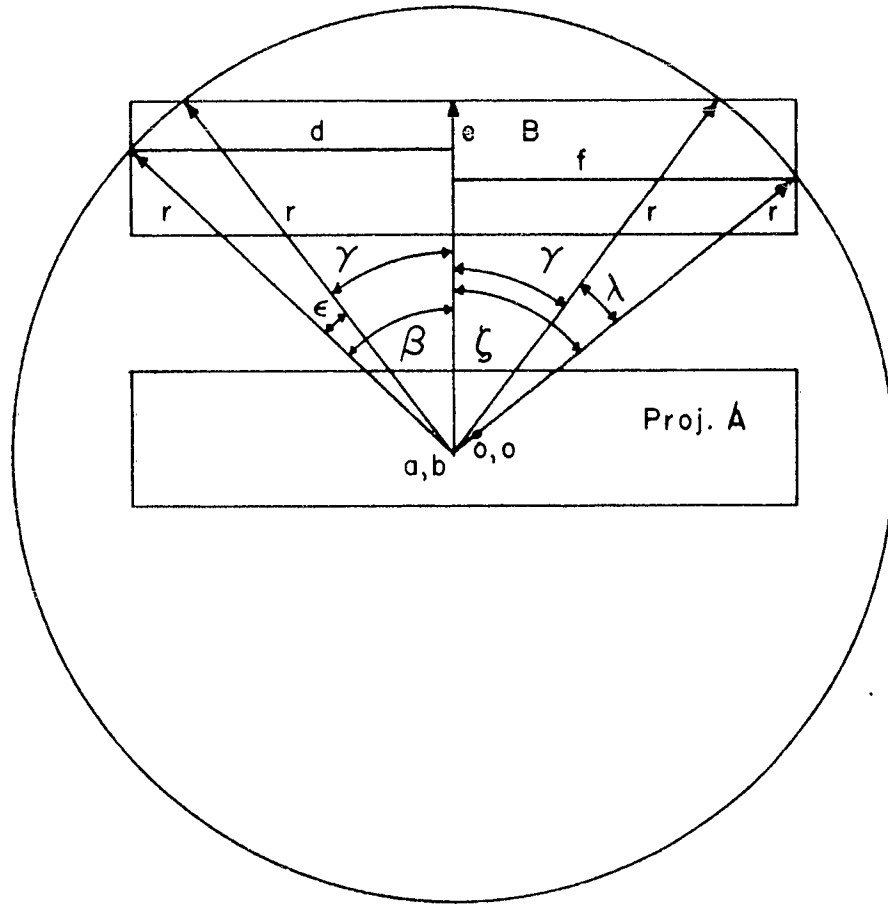$$\delta = \alpha - \gamma \quad , \quad \epsilon = \beta - \gamma \quad , \quad \phi = \delta + \epsilon$$

$$P(B)_E = \frac{\phi r}{2\pi r}$$

$$P(B)_E = \frac{1}{2\pi}\left[\cos^{-1}\left(\frac{z_o - b_o - b}{r}\right) + \sin^{-1}\left(\frac{a_o - a}{r}\right) - \cos^{-1}\left(\frac{z_o - b_o - b}{r}\right)\right]$$

Figure 17

$P(B)_F$ - Arc Intersects Slit B

Once on Upper Edge and

Once on Lower Edge

$$P(B)_F$$

$$\alpha = \cos^{-1}\left(\frac{c}{r}\right) \qquad , \qquad c = z_0 - b_0 - b$$

$$\gamma = \cos^{-1}\left(\frac{e}{r}\right) \qquad , \qquad e = z_0 + b_0 - b$$

$$\delta = \phi = \alpha - \gamma$$

$$P(B)_F = \frac{\phi r}{2\pi r}$$

$$P(B)_F = \frac{1}{2\pi}\left[\cos^{-1}\left(\frac{z_0 - b_0 - b}{r}\right) - \cos^{-1}\left(\frac{z_0 - b_0 - b}{r}\right)\right]$$

Figure 18

$P(B)_G$ - Arc Intersects Slit B

Twice on Upper Edge and

Once on Each Side

$$\gamma = \cos^{-1}\left(\frac{e}{r}\right) \qquad , \qquad e = z_0 + b_0 - b$$

$$\beta = \sin^{-1}\left(\frac{d}{r}\right) \qquad , \qquad d = a_0 - a$$

$$\zeta = \sin^{-1}\left(\frac{f}{r}\right) \qquad , \qquad f = a_0 + a$$

$$\epsilon = \beta - \gamma \quad , \quad \lambda = \zeta - \gamma \quad , \quad \phi = \epsilon + \lambda$$
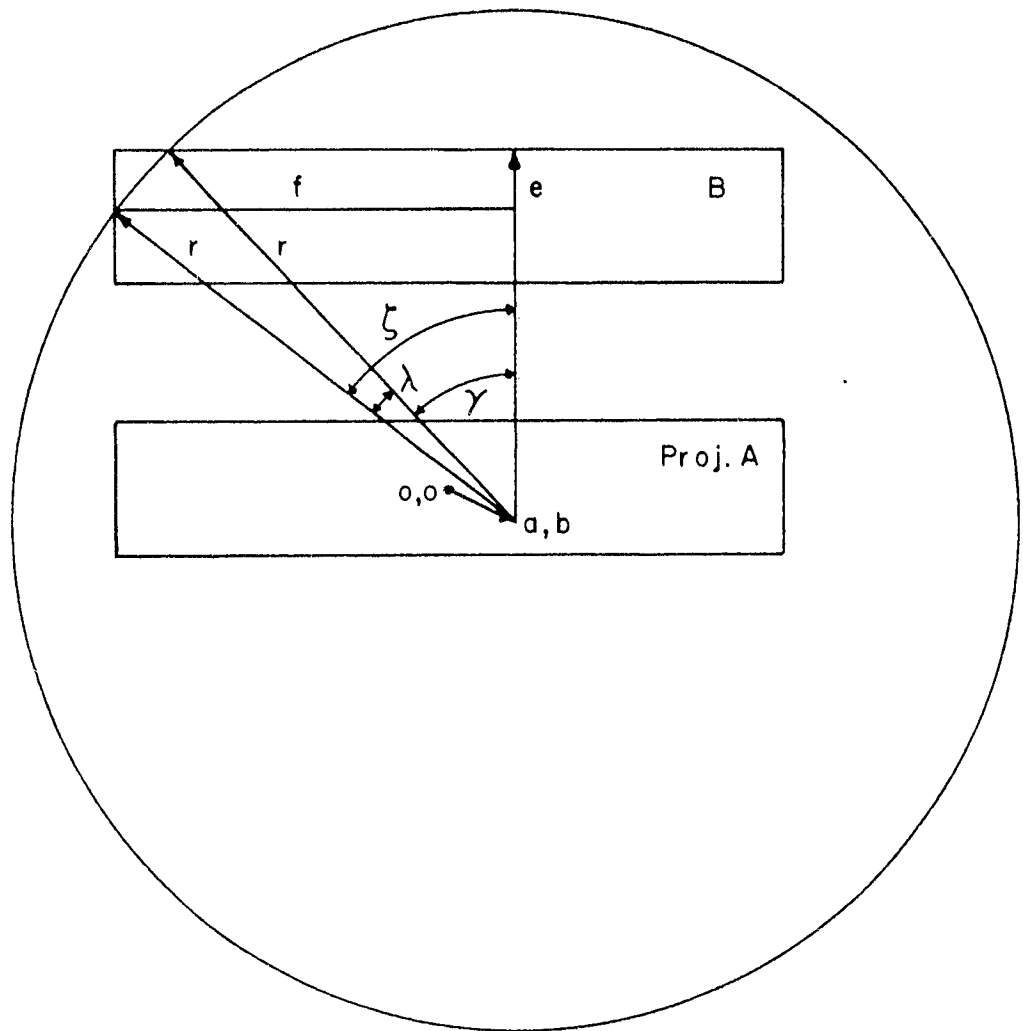
$$P(B)_G = \frac{\phi r}{2\pi r}$$

$$P(B)_G = \frac{1}{2\pi}\left[\sin^{-1}\left(\frac{a_0 - a}{r}\right) + \sin^{-1}\left(\frac{a_0 + a}{r}\right) - \cos^{-1}\left(\frac{z_0 + b_0 - b}{r}\right)\right]$$

Figure 19

$P(B)_H$ - Arc Intersects Slit B

Once on Upper Edge and

On One Side

$$\gamma = \cos^{-1}\left(\frac{e}{r}\right) \quad , \quad e = .z_0 + b_0 - b$$

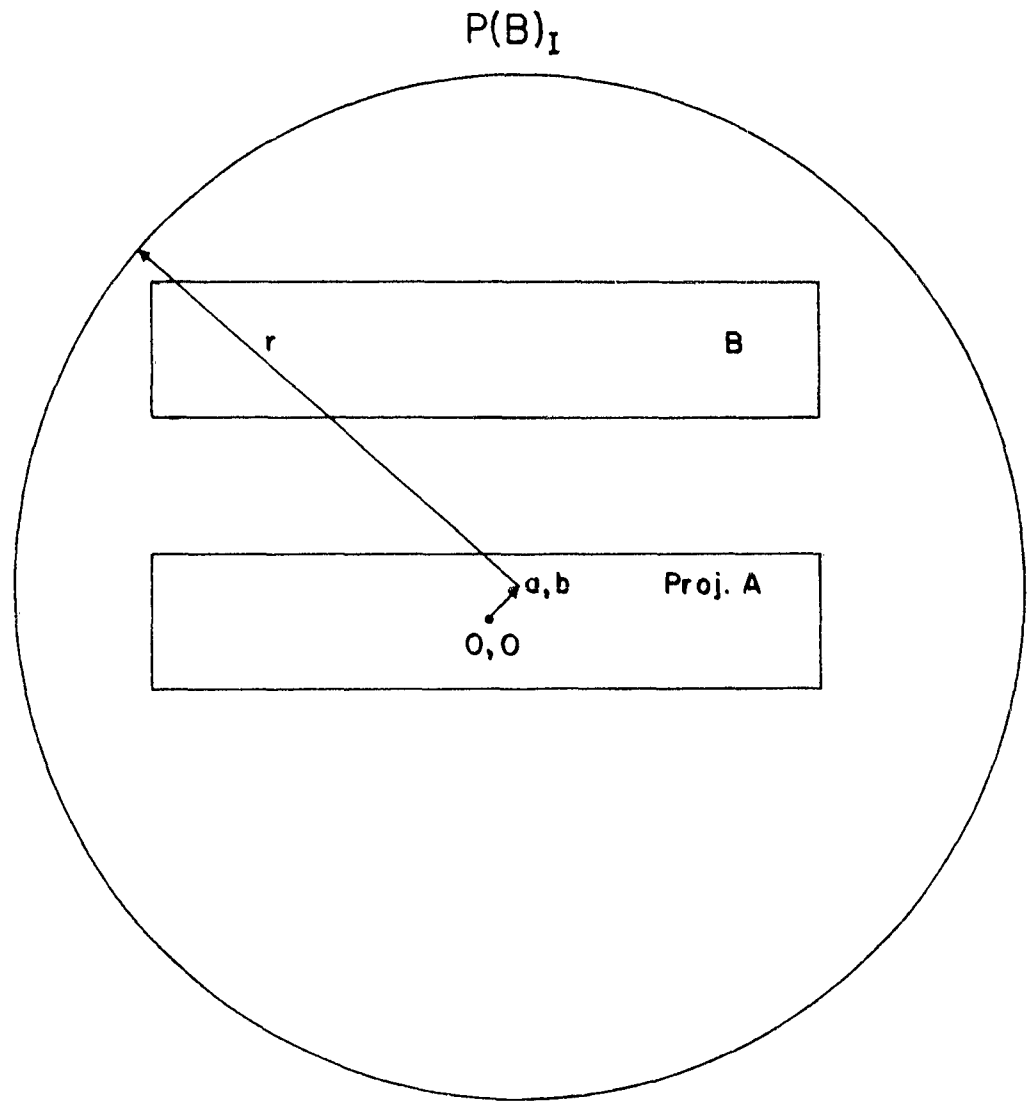$$\zeta = \sin^{-1}\left(\frac{f}{r}\right) \quad , \quad f = a_0 + a$$

$$\lambda = \zeta - \gamma \quad , \quad \phi = \lambda$$

$$P(B)_H = \frac{\phi r}{2\pi r}$$

$$P(B)_H = \frac{1}{2\pi}\left[\sin^{-1}\left(\frac{a_0 + a}{r}\right) - \cos^{-1}\left(\frac{z_0 + b_0 - b}{r}\right)\right]$$

Figure 20

$P(B)_I$ - No Arc Falls Within Slit B

$$P(B)_I = \frac{0}{2\pi r} = 0$$

For each value of θ_0, it is necessary to divide θ into nine ranges in order to integrate equation 27. Each of these ranges includes one or more of the special cases of P(B). It is possible to calculate R(θ, θ_0) using only the approximations of equations 22, 23 and 24 for six of the ranges of θ. These ranges are found to be more than sufficient to define the important portion of the resolution curve.

In the following equations, r, z_0, b_0, a_0 are measured in milliradians so that r corresponds to θ and z_0 corresponds to θ_0. Also let $M = a_0 - \sqrt{r^2 - c^2}$, $N = a_0 - \sqrt{r^2 - e^2}$, and $C = \frac{1}{2\pi r_0^2}$. For $r \leq z_0 - 2b_0$:

$$R(\theta, \theta_0)_{I} = C \int_{-b_0}^{b_0} \int_{0}^{a_0} P(B)_A \, da \, db \tag{28}$$

For $z_0 - 2b_0 \leq r \leq z_0$:

$$R(\theta, \theta_0)_{II} = C \int_{-b_0}^{z_0 - b_0 - r} \int_{0}^{a_0} P(B)_A \, da \, db$$

$$+ C \int_{z_0 - b_0 - r}^{b_0} \int_{0}^{M} P(B)_B \, da \, db \tag{29}$$

$$+ C \int_{z_0 - b_0 - r}^{b_0} \int_{M}^{a_0} P(B)_C \, da \, db$$

For $z_0 \leq r \leq z_0 + 2b_0$:

$$R(\theta,\theta_0)_{III} = C \int_{-b_0}^{z_0+b_0-r} \int_0^M P(B)_B \, da \, db + C \int_{-b_0}^{z_0+b_0-r} \int_M^{a_0} P(B)_C \, da \, db$$

$$+ C \int_{z_0+b_0-r}^{b_0} \int_0^M P(B)_D \, da \, db + C \int_{z_0+b_0-r}^{b_0} \int_M^N P(B)_E \, da \, db + C \int_{z_0+b_0-r}^{b_0} \int_N^{a_0} P(B)_F \, da \, db$$

$$(30)$$

For $z_0 + 2b_0 \leq r \leq \sqrt{(z_0-2b_0)^2 + a_0^2}$:

$$R(\theta,\theta_0)_{IV} = C \int_{-b_0}^{b_0} \int_0^M P(B)_D \, da \, db + C \int_{-b_0}^{b_0} \int_M^N P(B)_E \, da \, db$$

$$+ C \int_{-b_0}^{b_0} \int_N^{a_0} P(B)_F \, da \, db$$

$$(31)$$

For $\sqrt{(z_0-2b_0)^2 + (2a_0)^2} \leq r \leq \sqrt{z_0^2 + (2a_0)^2}$:

$$R(\theta,\theta_0)_{VIII} = C \int_{-b_0}^{b_0} \int_{\sqrt{r^2-e^2}-a_0}^{a_0} P(B)_H \, da \, db + C \int_{-b_0}^{b_0} \int_0^{\sqrt{r^2-e^2}-a_0} P(B)_I \, da \, db$$

$$(32)$$

For $\sqrt{(z_0+2b_0)^2 + (2a_0)^2} \leq r$:

$$R(\theta,\theta_0)_{IX} = C \int_{-b_0}^{b_0} \int_0^{a_0} P(B)_I \, da \, db$$

$$(33)$$

There are three ranges of r between $\sqrt{(Z_0 - 2b_0)^2 + \partial_0^2}$ and

$\sqrt{(Z_0 - 2b_0)^2 + (2\partial_0)^2}$ that contribute nothing of

interest to the $R(\theta, \theta_0)$ curve and since they are diffi-

cult to evaluate they will be neglected.

Since $P(B)_A = 0$, the first range of r gives a value

of zero for $R(\theta, \theta_0)_I$. Similarly, since $P(B)_I = 0$, the

last range of r gives a value of zero for $R(\theta, \theta_0)_{IX}$. The

complete calculation of $R(\theta, \theta_0)_{IV}$ is shown in the

Appendix. The same type integrals with different limits

also had to be evaluated for the other ranges of r. These

calculations give the following expressions for $R(\theta, \theta_0)$.

For $r \leq Z_0 - 2b_0$:

$$R(\theta, \theta_0)_I = 0$$

(34)

For $Z_0 - 2b_0 \leq r \leq Z_0$:

$$R(\theta, \theta_0)_{II} = \frac{\partial_0 r}{2\pi^2 r_0^2}\left[\sqrt{1-\alpha^2} - \alpha \cos^{-1}\alpha\right] - \frac{1}{8\pi^2 r_0^2}\left(2b_0 - Z_0 + r\right)^2$$

(35)

For $Z_0 \leq r \leq Z_0 + 2b_0$:

$$R(\theta, \theta_0)_{III} = \frac{1}{8\pi^2 r_0^2}\left(r^2 + Z_0^2 - 2rZ_0 - 4b_0^2 + 4b_0 Z_0 - 4rb_0\right)$$

$$+ \frac{r\partial_0}{2\pi^2 r_0^2}\left[\sqrt{1-\alpha^2} - \alpha \cos^{-1}\alpha + 2\gamma\cos^{-1}\gamma - 2\sqrt{1-\gamma^2}\right]$$ (36)

For $Z_0 + 2b_0 \leq r \leq \sqrt{(Z_0 - 2b_0)^2 + a_0^2}$:

$$R(\theta, \theta_0)_{IV} = \frac{ra_0}{2\pi^2 r_0^2}\left[2\gamma\cos^{-1}\gamma - 2\sqrt{1-\gamma^2} - \alpha\cos^{-1}\alpha + \sqrt{1-\alpha^2} - \delta\cos^{-1}\delta + \sqrt{1-\delta^2}\right]$$

$$- \frac{b_0^2}{\pi^2 r_0^2}$$

(37)

For $\sqrt{(Z_0 - 2b_0)^2 + (2a_0)^2} \leq r \leq \sqrt{Z_0^2 + (2a_0)^2}$:

$$R(\theta, \theta_0)_{VIII} = \frac{b_0 r}{2\pi^2 r_0^2}\left[\frac{2a_0}{r}\sin^{-1}\frac{2a_0}{r} + \sqrt{1 - \left(\frac{2a_0}{r}\right)^2}\right]$$

$$- \frac{b_0 Z_0}{2\pi^2 r_0^2} - \frac{b_0^2}{2\pi^2 r_0^2}$$

$$+ \frac{ra_0}{2\pi^2 r_0^2}\left[\gamma\cos^{-1}\gamma - \sqrt{1-\gamma^2} - \delta\cos^{-1}\delta + \sqrt{1-\delta^2}\right]$$

(38)

For $\sqrt{(Z_0 + 2b_0)^2 + (2a_0)^2} \leq r$

$$R(\theta, \theta_0)_{IX} = 0$$

(39)

In Figure 21, the resolution function is plotted for a_0 = 6.35 milliradians, b_0 = .2 milliradians, r_0 = 1000 milliradians, and z_0 = .6 milliradians and 3.6 milliradians to show how the function varies for different positions (z_0) of the movable slit. These values of the parameters correspond to an apparatus with slits one inch long by .016 inches wide and each slit a distance of 2

meters from the target. The resolution function is plotted in Figure 22 for an apparatus with 8 inch long slits when z_0 is again .6 milliradians and 3.6 milliradians. Figure 23 shows the z_0 = .6 milliradian curves of both Figure 21 and Figure 22 plotted on the same scale to compare areas and Figure 24 shows the z_0 = .6 milliradian curves of both Figure 21 and Figure 22 with the maximum points normalized to compare shapes.

No attempt was made to generalize the resolution function to include targets of finite size. This can probably be done satisfactorily by employing the methods of numerical integration and will certainly broaden the curves. The generalized resolution curves for each position of the movable slit can then be used to correct the raw data using the general method developed by Eckart[16].

The corrected coincidence counting rate at θ is proportional to the total number of annihilation pairs per unit time having a P_ρ component of momentum. The relation is

$$D(P_\rho) = const. \int_0^\infty \int_0^{2\pi} \rho(P) P_\rho \, d\phi \, dP_y \tag{40}$$

where

$$P_\rho = \sqrt{P_x^2 + P_z^2} \tag{41}$$

16
   Eckart, C. op. cit.

Figure 21

Resolution Curves for Method B

θ_o = 0.6 mrad. and 3.6 mrad.

a_o = 6.35 mrad.

RESOLUTION CURVES

$\theta_o = 0.6$ mr.

$\theta_o = 3.6$ mr.

$R(\theta, \theta_o)$

θ (MR.)
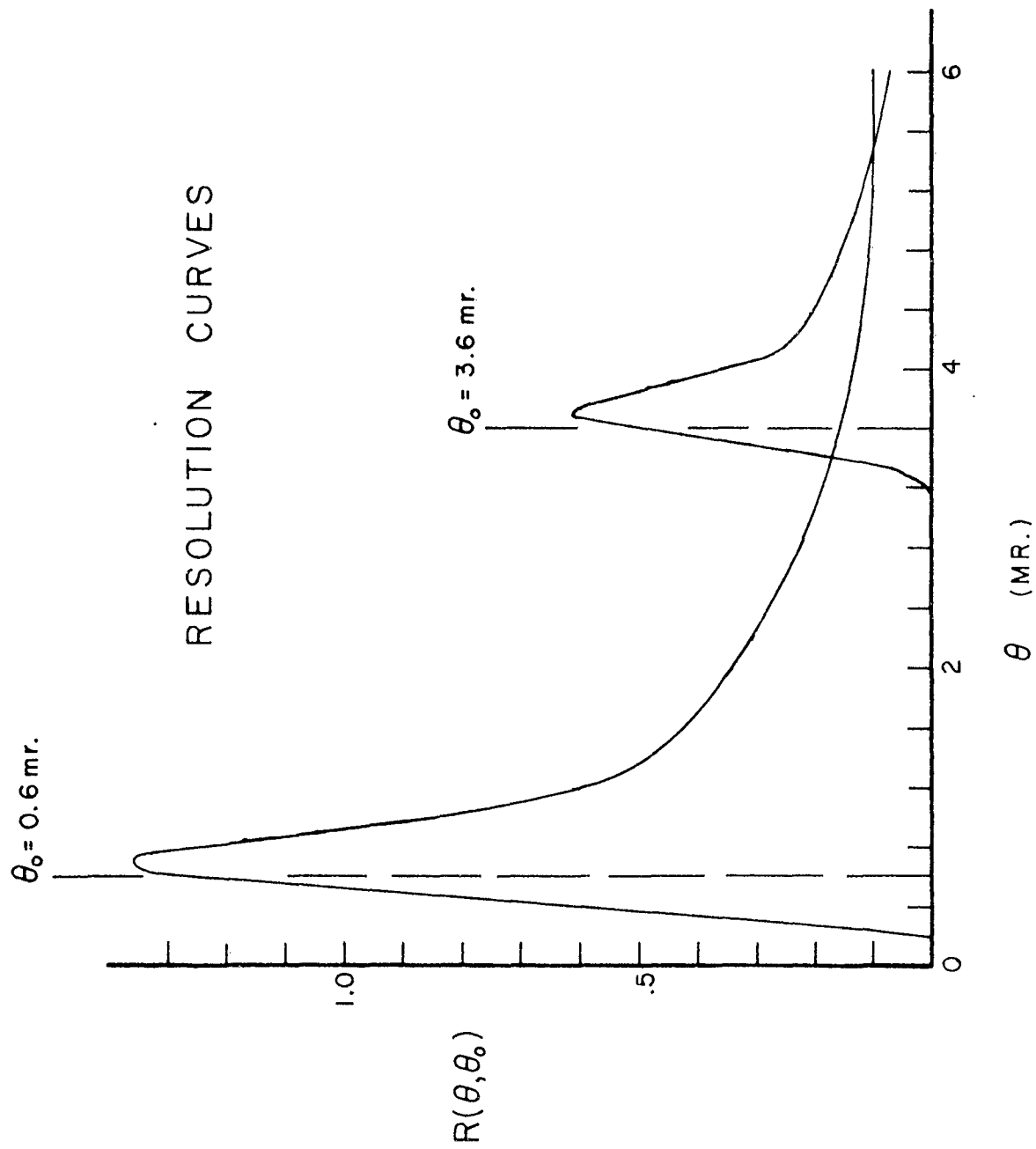
Figure 22

Resolution Curves for Method B

θ_o = 0.6 mrad. and 3.6 mrad.

a_o = 50.5 mrad.

RESOLUTION CURVES

$\theta_o = 0.6$ mr.

$\theta_o = 3.6$ mr.

$R(\theta, \theta_o)$

10

5

0   2   4   6

θ ´ (MR.)
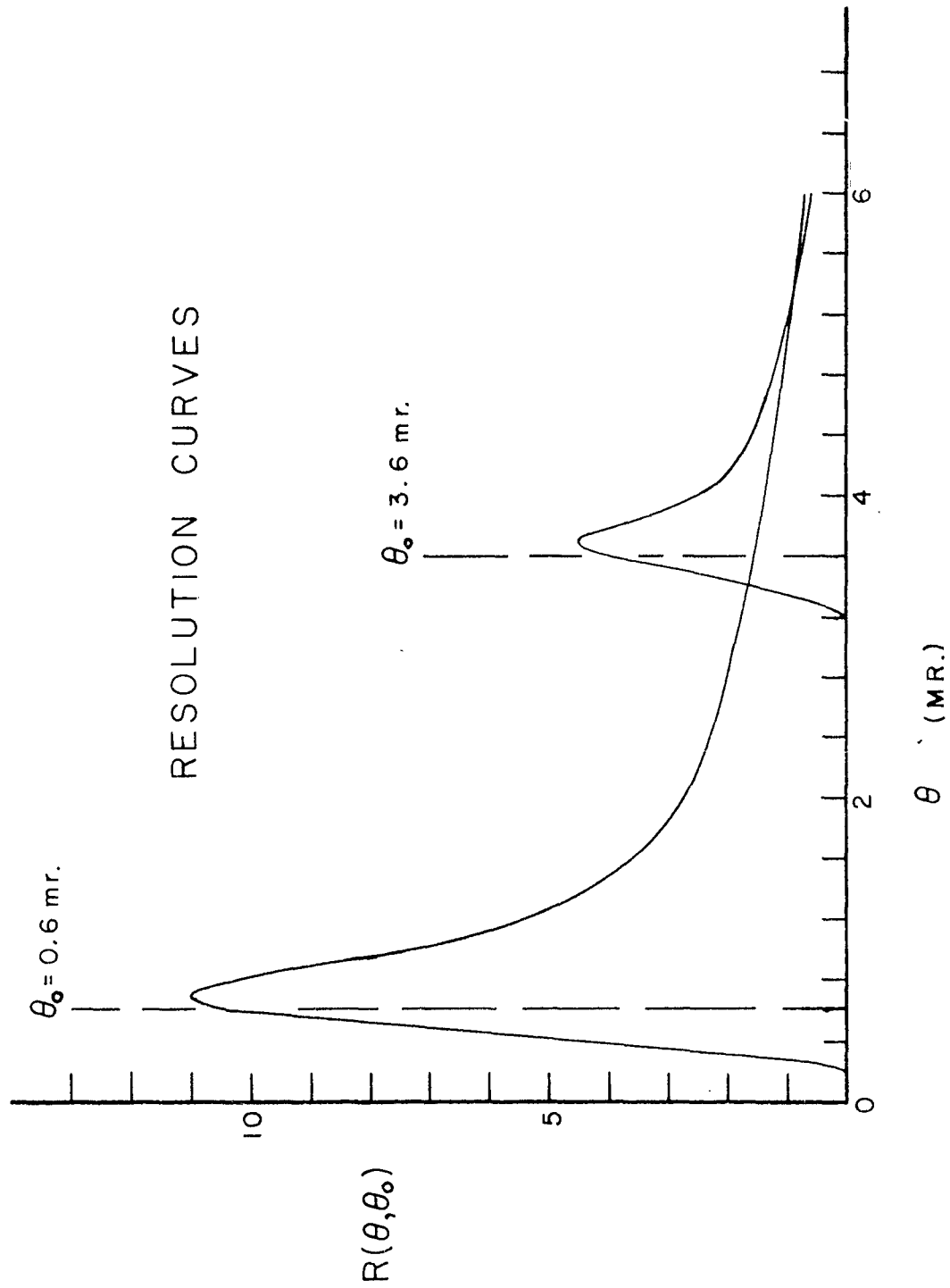
Figure 23

Resolution Curves for Method B

θ_o = 0.6 mrad.
a_o = 6.35 mrad. and 50.5 mrad.

(Drawn to Scale)

RESOLUTION CURVES

$\theta_o = 0.6\,mr.$

$a_o = 50.5\,mr.$

$a_o = 6.35\,mr.$

$R(\theta,\theta_o)$

θ (MR.)
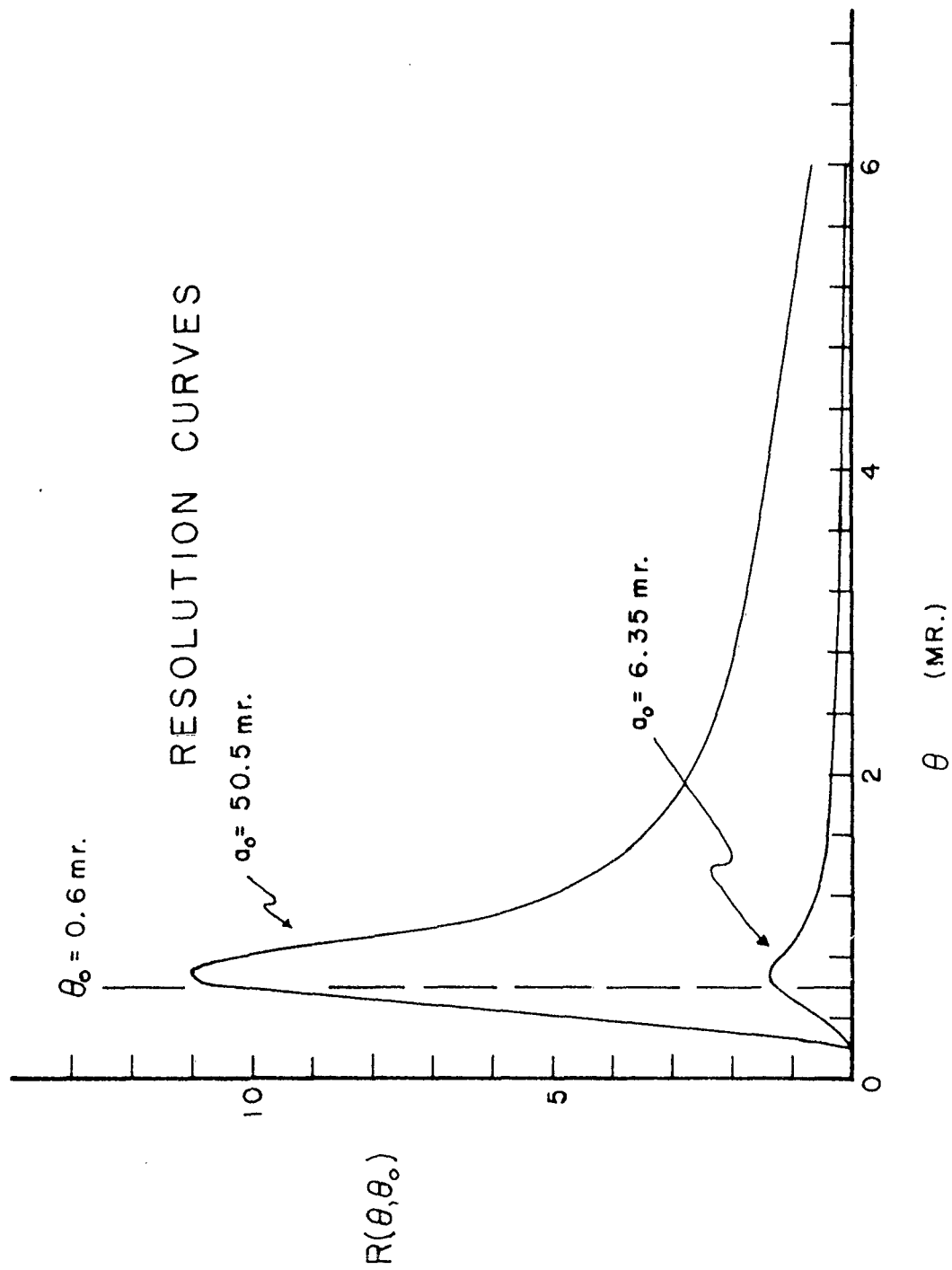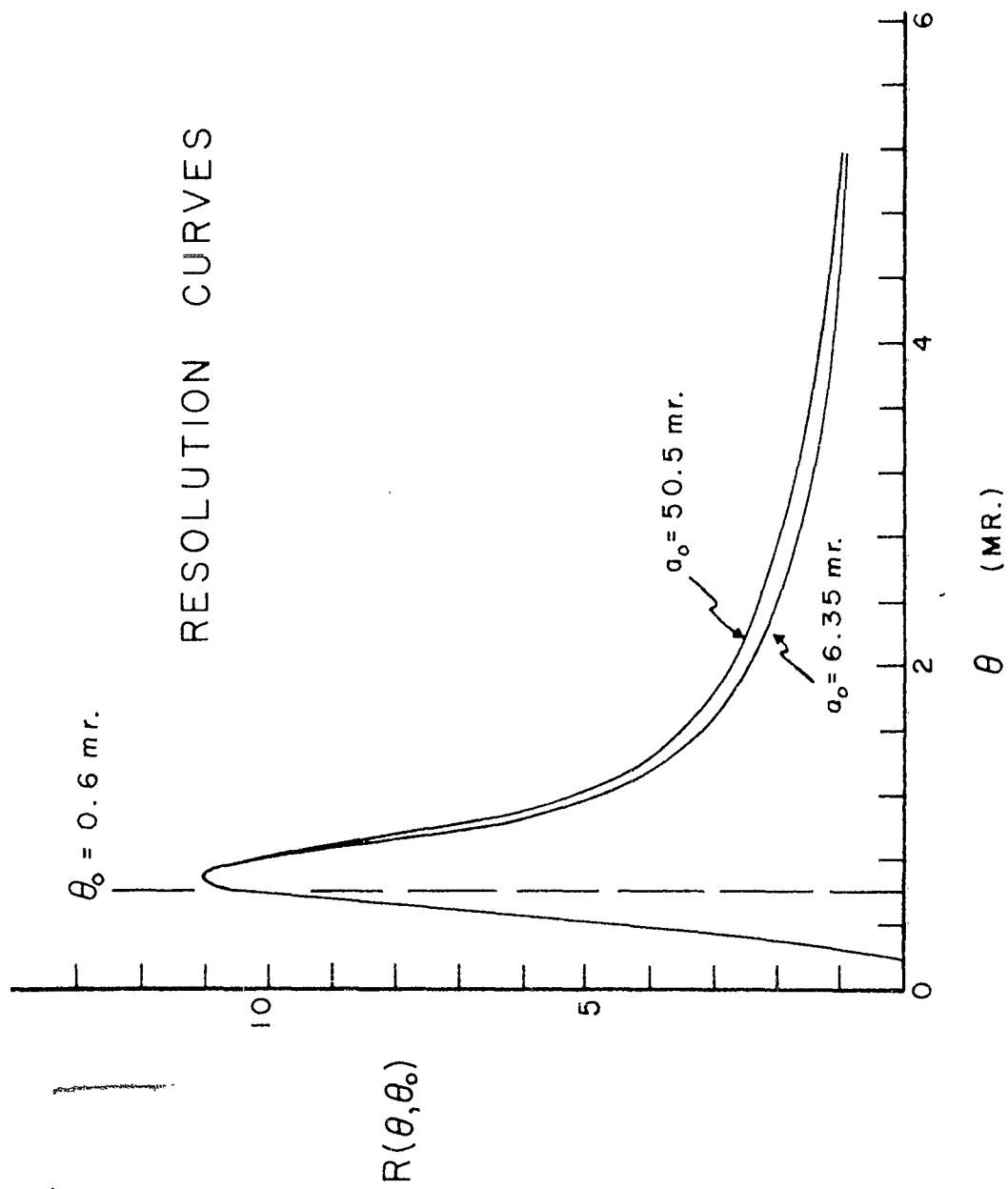
Figure 24

Resolution Curves for Method B

θ_O = 0.6 mrad.

a_O = 6.35 mrad. and 50.5 mrad.

(Normalized so that the Maximum Points are Equal)

RESOLUTION CURVES

$\theta_o = 0.6$ mr.

$a_o = 50.5$ mr.

$a_o = 6.35$ mr.

$R(\theta, \theta_o)$

θ (MR.)

Equation 40 can be written as

$$\frac{D(P_\rho)}{P_\rho} = const. \int_0^\infty \int_0^{2\pi} \rho(P) \, d\phi \, dP_y$$

(42)

Since an isotropic momentum distribution has been assumed, equation 42 can be integrated over ϕ to get

$$\frac{D(P_\rho)}{P_\rho} = const. \, 2\pi \int_0^\infty \rho(P) \, dP_y$$

(43)

From this relation Bahena[17] has shown that the distribution of momentum is given by

$$N(P) = N(P_z) = const. \, P^2 \int_0^\infty \frac{1}{\theta} \frac{dD(\theta)}{d\theta} \, dP_x$$

(44)

where

$$\theta = \frac{r}{r_0} = \frac{P_\rho}{mc}$$

(45)

17
   Millett, W. E., and Castillo-Bahena, R., op. cit.

CHAPTER III

EVALUATION AND COMPARISON OF METHODS

A. Speed in Taking Data

The study of the angular correlation of annihilation
radiation is always a rather time-consuming experiment
since the solid angles utilized by the crystal scintil-
lators have to be very small, of the order of 10^{-5} stera-
dians. The decay of the source, the possibility of the
apparatus getting knocked out of alignment while taking
data, and drift in the electronic circuits make it ad-
visable to collect the data in as short a time as possible.
This becomes even more desirable if the target is being
held at low temperature or under a vacuum.

The factor of speed in taking data is the big advan-
tage of the multiple coincidence channel apparatus. If
four properly spaced slits are used at each end of the
apparatus, it is possible to collect data for 16 angles
in the same time that a single coincidence channel appa-
ratus with the same size slits requires for one angle.
The data must be taken with frequent change of the angle
between the two sets of slits, however, because the re-
sponse of a single channel can vary slightly due to

75

electronic drift and temperature changes, so that the sensitivity cannot be considered as constant from day to day. By changing the position of the movable slits stepwise up and down again, part of a coincidence curve is obtained for each counter pair. Independently of single channel sensitivities, these 16 curves can then be joined together to make one curve.

The usual arrangement of the photomultiplier tubes and slits[18,19] in this type apparatus restrict the maximum length of the slits to about 2 inches. No such restriction exists for the single coincidence channel apparatus; so it is possible to use slits much greater than 2 inches long and thereby reduce the counting time advantage of the multiple coincidence channel apparatus.

B. Structural Complexity

The SCC apparatus (single coincidence channel) is easier to construct than the MCC apparatus (multiple coincidence channel). The MCC apparatus requires the construction of four times as many precision slits and photomultiplier tube supports. The design of the lead shielding is necessarily more complicated.

C. Electronic Components

The MCC apparatus requires far more circuitry than the SCC apparatus. It requires four times as many tube bases, preamplifiers, and pulse shapers; sixteen times

[18]Trumpy, G., op. cit.
[19]Lovseth, j., op. cit.

as many coincidence circuits; and a complex switch for directing the output of each coincidence circuit to the correct sequence of registers.

D. Expense

The MCC apparatus costs more to build than the SCC apparatus. It requires more photomultiplier tubes, far more electronic equipment, and far more man-hours to construct.

E. Alignment

The MCC apparatus is harder to align than the SCC apparatus. Eight slits have to be adjusted as opposed to just two for the single coincidence channel apparatus.

F. Analysis of Data

It is much easier to correct the data for instrumental resolution by Method A because the resolution curve is symmetrical and is the same for all positions of the movable slit, while the resolution curve for Method B is asymmetrical and varies greatly with the position of the movable slit. (Compare Figure 11 with Figures 21 and 22.) It is also much easier to obtain the momentum distribution by Method A because it only involves the determination of slopes as opposed to the determination of areas required by Method B.

In order to Use Method A, however, it is necessary that the effective slit length be much greater than 10 milliradians. As stated earlier, the maximum slit length that can be used in the multiple coincidence

channel apparatus is about 2 inches which corresponds to about 25 milliradians at a distance of 2 meters. In order to fit a standard photomultiplier tube and still cover the length of the slit, the scintillators are usually cut in the shape of short right cylinders. This means that the efficiency of the counter drops from a maximum at the center of the slit to zero at each edge which reduces the effective slit length by about half and invalidates the use of equation 21 which assumes a constant crystal efficiency.

With a maximum effective slit length of about 12.5 milliradians, the use of Method A to analyze the data obtained by a multiple coincidence channel apparatus is not entirely justified. Several alternatives exist: 1) use Method B to evaluate the data; 2) devise a way to use longer slits with the multiple coincidence channel apparatus; 3) collect the data with a long slit single coincidence channel apparatus and use either or both methods to analyze the data; and 4) devise a method (for varying crystal efficiency) of relating the count rate to the momentum distribution from equation 21.

At the present, alternative 3 appears to be the best method.

APPENDIX

The complete calculation of $R(\theta, \theta_0)_{\overline{W}}$.

For $z_0 + 2b_0 \le r \le \sqrt{(z_0 - 2b_0)^2 + \partial_0^2}$.

$$R(\theta, \theta_0)_{\overline{W}} = c \int_{-b_0}^{b_0} \int_0^M P(B)_D \, d\partial \, db + c \int_{-b_0}^{b_0} \int_M^N P(B)_E \, d\partial \, db + c \int_{-b_0}^{b_0} \int_N^{\partial_0} P(B)_F \, d\partial \, db$$

(A-1)

Each of these integrals will be calculated separately and the results added. The integral for $P(B)_D$ is

$$c \int_{-b_0}^{b_0} \int_0^M P(B)_D \, d\partial \, db = c \int_{-b_0}^{b_0} \int_0^{\partial_0 - \sqrt{\hbar^2 - c^2}} \frac{1}{\pi} \cos^{-1} \frac{c}{r} \, d\partial \, db - c \int_{-b_0}^{b_0} \int_0^{\partial_0 - \sqrt{\hbar^2 - c^2}} \frac{1}{\pi} \cos^{-1} \frac{e}{r} \, d\partial \, db$$

(A-2)

Integrating over the variable a gives

$$c \int_{-b_0}^{b_0} \int_0^M P(B)_D \, d\partial \, db = \frac{c}{\pi} \int_{-b_0}^{b_0} \partial_0 \cos^{-1} \frac{c}{r} \, db - \frac{cr}{\pi} \int_{-b_0}^{b_0} \sqrt{1 - \left(\frac{c}{r}\right)^2} \cos^{-1} \frac{c}{r} \, db$$

$$+ \frac{cr}{\pi} \int_{-b_0}^{b_0} \sqrt{1 - \left(\frac{c}{r}\right)^2} \cos^{-1} \frac{e}{r} \, db - \frac{c}{\pi} \int_{-b_0}^{b_0} \partial_0 \cos^{-1} \frac{e}{r} \, db$$

(A-3)

The integral for $P(B)_E$ is

$$c \int_{-b_0}^{b_0} \int_M^N P(B)_E \, d\partial \, db = c \int_{-b_0}^{b_0} \int_M^N \frac{1}{2\pi} \cos^{-1} \frac{c}{r} \, d\partial \, db + c \int_{-b_0}^{b_0} \int_M^N \frac{1}{2\pi} \sin^{-1}\left(\frac{\partial_0 - \partial}{r}\right) d\partial \, db$$

$$- c \int_{-b_0}^{b_0} \int_M^N \frac{1}{\pi} \cos^{-1} \frac{e}{r} \, d\partial \, db \qquad \text{(A-4)}$$

79

Let these integrals be called I, II, and III respectively.

$$I = \frac{c}{2\pi} \int_{-b_o}^{b_o} \int_{a_o - \sqrt{r^2 - c^2}}^{a_o - \sqrt{r^2 - e^2}} \cos^{-1} \frac{c}{r} \, da \, db \tag{A-5}$$

Integrating over the variable a gives

$$I = -\frac{cr}{2\pi} \int_{-b_o}^{b_o} \sqrt{1 - \left(\frac{e}{r}\right)^2} \cos^{-1} \frac{c}{r} \, db + \frac{cr}{2\pi} \int_{-b_o}^{b_o} \sqrt{1 - \left(\frac{c}{r}\right)^2} \cos^{-1} \frac{c}{r} \, db \tag{A-6}$$

Integral II is

$$II = \frac{c}{2\pi} \int_{-b_o}^{b_o} \int_{a_o - \sqrt{r^2 - c^2}}^{a_o - \sqrt{r^2 - e^2}} \sin^{-1} \left(\frac{a_o - a}{r}\right) \, db \, da \tag{A-7}$$

Let $A = \frac{a_o - a}{r}$ so $da = -r \, dA$.

When $a = a_o - \sqrt{r^2 - e^2}$, $A = \frac{\sqrt{r^2 - e^2}}{r}$ and when $a = a_o - \sqrt{r^2 - c^2}$,

$A = \frac{\sqrt{r^2 - c^2}}{r}$, so integral II becomes

$$II = -\frac{cr}{2\pi} \int_{-b_o}^{b_o} \int_{\frac{\sqrt{r^2 - c^2}}{r}}^{\frac{\sqrt{r^2 - e^2}}{r}} \sin^{-1} A \, dA \tag{A-8}$$

Integrating over the variable A gives

$$II = -\frac{cr}{2\pi} \int_{-b_o}^{b_o} \frac{2b_o}{r} \, db - \frac{cr}{2\pi} \int_{-b_o}^{b_o} \sqrt{1 - \left(\frac{e}{r}\right)^2} \sin^{-1} \sqrt{1 - \left(\frac{e}{r}\right)^2} \, db$$
$$+ \frac{cr}{2\pi} \int_{-b_o}^{b_o} \sqrt{1 - \left(\frac{c}{r}\right)^2} \sin^{-1} \sqrt{1 - \left(\frac{c}{r}\right)^2} \, db \tag{A-9}$$

Integral III is

$$III = -\frac{C}{\pi}\int_{-b_o}^{b_o}\int_{a_o-\sqrt{r^2-c^2}}^{a_o-\sqrt{r^2-e^2}} cos^{-1}\frac{e}{r}\,da\,db$$

(A-10)

Integrating over the variable a gives

$$III = \frac{Cr}{\pi}\int_{-b_o}^{b_o}\sqrt{1-\left(\frac{e}{r}\right)^2}cos^{-1}\frac{e}{r}\,db - \frac{Cr}{\pi}\int_{-b_o}^{b_o}\sqrt{1-\left(\frac{c}{r}\right)^2}cos^{-1}\frac{e}{r}\,db$$

(A-11)

The total integral for $P(B)_E$ is then

$$C\int_{-b_o}^{b_o}\int_{M}^{N}P(B)_E\,da\,db = -\frac{Cr}{2\pi}\int_{-b_o}^{b_o}\sqrt{1-\left(\frac{e}{r}\right)^2}cos^{-1}\frac{c}{r}\,db$$

$$+ \frac{Cr}{2\pi}\int_{-b_o}^{b_o}\sqrt{1-\left(\frac{c}{r}\right)^2}cos^{-1}\frac{c}{r}\,db - \frac{Cr}{2\pi}\int_{-b_o}^{b_o}\frac{2b_o}{r}\,db$$

$$- \frac{Cr}{2\pi}\int_{-b_o}^{b_o}\sqrt{1-\left(\frac{e}{r}\right)^2}sin^{-1}\sqrt{1-\left(\frac{e}{r}\right)^2}\,db + \frac{Cr}{2\pi}\int_{-b_o}^{b_o}\sqrt{1-\left(\frac{c}{r}\right)^2}sin^{-1}\sqrt{1-\left(\frac{c}{r}\right)^2}\,db$$

$$+ \frac{Cr}{\pi}\int_{-b_o}^{b_o}\sqrt{1-\left(\frac{e}{r}\right)^2}cos^{-1}\frac{e}{r}\,db - \frac{Cr}{\pi}\int_{-b_o}^{b_o}\sqrt{1-\left(\frac{c}{r}\right)^2}cos^{-1}\frac{e}{r}\,db$$

(A-12)

The integral for $P(B)_F$ is

$$C\int_{-b_o}^{b_o}\int_{N}^{a_o}P(B)_F\,da\,db = C\int_{-b_o}^{b_o}\int_{a_o-\sqrt{r^2-e^2}}^{a_o}\frac{1}{2\pi}cos^{-1}\frac{c}{r}\,db\,da - C\int_{-b_o}^{b_o}\int_{a_o-\sqrt{r^2-e^2}}^{a_o}\frac{1}{2\pi}cos^{-1}\frac{e}{r}\,db\,da$$

(A-13)

Integrating over the variable a gives

$$C\int_{-b_o}^{b_o}\int_{N}^{a_o} P(B)_F \, da \, db = \frac{Cr}{2\pi}\int_{-b_o}^{b_o}\sqrt{1-\left(\frac{c}{r}\right)^2}\cos^{-1}\frac{c}{r}\,db - \frac{Cr}{2\pi}\int_{-b_o}^{b_o}\sqrt{1-\left(\frac{e}{r}\right)^2}\cos^{-1}\frac{e}{r}\,db$$

(A-14)

Therefore, the total expression for $R(\theta,\theta_o)_{\mathrm{IV}}$ is

$$R(\theta,\theta_o)_{\mathrm{IV}} = \frac{C}{\pi}\int_{-b_o}^{b_o}a_o\cos^{-1}\frac{c}{r}\,db - \frac{Cr}{\pi}\int_{-b_o}^{b_o}\sqrt{1-\left(\frac{c}{r}\right)^2}\cos^{-1}\frac{c}{r}\,db$$

$$+ \frac{Cr}{\pi}\int_{-b_o}^{b_o}\sqrt{1-\left(\frac{c}{r}\right)^2}\cos^{-1}\frac{e}{r}\,db - \frac{C}{\pi}\int_{-b_o}^{b_o}a_o\cos^{-1}\frac{e}{r}\,db$$

$$- \frac{Cr}{2\pi}\int_{-b_o}^{b_o}\sqrt{1-\left(\frac{e}{r}\right)^2}\cos^{-1}\frac{c}{r}\,db + \frac{Cr}{2\pi}\int_{-b_o}^{b_o}\sqrt{1-\left(\frac{c}{r}\right)^2}\cos^{-1}\frac{c}{r}\,db$$

$$- \frac{Cr}{2\pi}\int_{-b_o}^{b_o}\frac{2b_o}{r}\,db - \frac{Cr}{2\pi}\int_{-b_o}^{b_o}\sqrt{1-\left(\frac{e}{r}\right)^2}\sin^{-1}\sqrt{1-\left(\frac{e}{r}\right)^2}\,db$$

$$+ \frac{Cr}{2\pi}\int_{-b_o}^{b_o}\sqrt{1-\left(\frac{c}{r}\right)^2}\sin^{-1}\sqrt{1-\left(\frac{c}{r}\right)^2}\,db + \frac{Cr}{\pi}\int_{-b_o}^{b_o}\sqrt{1-\left(\frac{e}{r}\right)^2}\cos^{-1}\frac{e}{r}\,db$$

$$- \frac{Cr}{\pi}\int_{-b_o}^{b_o}\sqrt{1-\left(\frac{c}{r}\right)^2}\cos^{-1}\frac{e}{r}\,db$$

(A-15)

$$+ \frac{Cr}{2\pi}\int_{-b_o}^{b_o}\sqrt{1-\left(\frac{e}{r}\right)^2}\cos^{-1}\frac{c}{r}\,db - \frac{Cr}{2\pi}\int_{-b_o}^{b_o}\sqrt{1-\left(\frac{e}{r}\right)^2}\cos^{-1}\frac{e}{r}\,db$$

After cancellations, this becomes

$$R(\theta,\theta_0)_{\text{IV}} = \frac{C\partial_0}{\Pi}\int_{-b_0}^{b_0}\cos^{-1}\frac{c}{r}\,db - \frac{C\partial_0}{\Pi}\int_{-b_0}^{b_0}\cos^{-1}\frac{e}{r}\,db - \frac{Cr}{2\Pi}\int_{-b_0}^{b_0}\frac{2b_0}{r}\,db$$

$$- \frac{Cr}{2\Pi}\int_{-b_0}^{b_0}\sqrt{1-\left(\frac{c}{r}\right)^2}\cos^{-1}\frac{c}{r}\,db + \frac{Cr}{2\Pi}\int_{-b_0}^{b_0}\sqrt{1-\left(\frac{e}{r}\right)^2}\cos^{-1}\frac{e}{r}\,db$$

$$- \frac{Cr}{2\Pi}\int_{-b_0}^{b_0}\sqrt{1-\left(\frac{e}{r}\right)^2}\sin^{-1}\sqrt{1-\left(\frac{e}{r}\right)^2}\,db$$

$$+ \frac{Cr}{2\Pi}\int_{-b_0}^{b_0}\sqrt{1-\left(\frac{c}{r}\right)^2}\sin^{-1}\sqrt{1-\left(\frac{c}{r}\right)^2}\,db \qquad \text{(A-16)}$$

Let these integrals be numbered I through VII respectively.

$$\text{I} = \frac{C\partial_0}{\Pi}\int_{-b_0}^{b_0}\cos^{-1}\left(\frac{z_0-b_0-b}{r}\right)db \qquad \text{(A-17)}$$

Let $A = \frac{z_0-b_0-b}{r}$ so $db = -r\,dA$

When $b = b_0$, $A = \frac{z_0-2b_0}{r} = \alpha$ and when $b = -b_0$,

$A = \frac{z_0}{r} = \gamma$, so integral I becomes

$$\text{I} = -\frac{C\partial_0 r}{\Pi}\int_{\gamma}^{\alpha}\cos^{-1}A\,dA = -\frac{C\partial_0 r}{\Pi}\left[A\cos^{-1}A - \sqrt{1-A^2}\right]_{\gamma}^{\alpha} \qquad \text{(A-18)}$$

$$\text{I} = -\frac{C\partial_0 r}{\Pi}\left[\alpha\cos^{-1}\alpha - \sqrt{1-\alpha^2} - \gamma\cos^{-1}\gamma + \sqrt{1-\gamma^2}\right] \qquad \text{(A-19)}$$

In a similar manner,

$$\text{II} = \frac{C\partial_0 r}{\pi}\left[\gamma\cos^{-1}\gamma - \sqrt{1-\gamma^2} - \delta\cos^{-1}\delta + \sqrt{1-\delta^2}\right] \qquad \text{(A-20)}$$

$$\text{III} = -\frac{Cr}{2\pi}\int_{-b_0}^{b_0}\frac{2b_0}{r}\,db = -\frac{2Cb_0^2}{\pi} \qquad \text{(A-21)}$$

$$\text{IV} = -\frac{Cr}{2\pi}\int_{-b_0}^{b_0}\sqrt{1-\left(\frac{c}{r}\right)^2}\,\cos^{-1}\frac{c}{r}\,db \qquad \text{(A-22)}$$

Let $\cos A = \frac{c}{r} = \frac{z_0 - b_0 - b}{r}$ so $db = r\sin A\,dA$.

When $b = b_0$, $A = \cos^{-1}\frac{z_0 - 2b_0}{r} = \cos^{-1}\alpha$ and when $b = -b_0$,

$A = \cos^{-1}\gamma$, so integral IV becomes

$$\text{IV} = -\frac{Cr^2}{2\pi}\int_{\cos^{-1}\gamma}^{\cos^{-1}\alpha} A\sin^2 A\,dA \qquad \text{(A-23)}$$

$$\text{IV} = -\frac{Cr^2}{2\pi}\left[\frac{A^2}{4} - \frac{A\sin 2A}{4} - \frac{\cos 2A}{8}\right]_{\cos^{-1}\gamma}^{\cos^{-1}\alpha} \qquad \text{(A-24)}$$

In a similar manner,

$$\text{V} = \frac{Cr^2}{2\pi}\left[\frac{A^2}{4} - \frac{A\sin 2A}{4} - \frac{\cos 2A}{8}\right]_{\cos^{-1}\delta}^{\cos^{-1}\gamma} \qquad \text{(A-25)}$$

$$\text{VI} = -\frac{Cr}{2\pi}\int_{-b_0}^{b_0}\sqrt{1-\left(\frac{e}{r}\right)^2}\,\sin^{-1}\sqrt{1-\left(\frac{e}{r}\right)^2}\,db \qquad \text{(A-26)}$$

Let $\cos A = \dfrac{e}{r} = \dfrac{z_0 + b_0 - b}{r}$ so $db = r \sin A \, dA$.

When $b = b_0$, $A = \cos^{-1} \gamma$ and when $b = -b_0$,
$A = \cos^{-1} \delta$, so integral VI becomes

$$\text{VI} = -\frac{Cr^2}{2\pi} \int_{\cos^{-1}\delta}^{\cos^{-1}\gamma} A \sin^2 A \, dA$$

(A-27)

$$\text{VI} = -\frac{Cr^2}{2\pi} \left[\frac{A^2}{4} - \frac{A \sin 2A}{4} - \frac{\cos 2A}{8} \right]_{\cos^{-1}\delta}^{\cos^{-1}\gamma}$$

(A-28)

In a similar manner,

$$\text{VII} = \frac{Cr^2}{2\pi} \left[\frac{A^2}{4} - \frac{A \sin 2A}{4} - \frac{\cos 2A}{8} \right]_{\cos^{-1}\gamma}^{\cos^{-1}\alpha}$$

(A-29)

Again there are possible cancellations in the expression
for $R(\theta, \theta_0)_{IV}$ and the final result is

$$R(\theta, \theta_0)_{IV} = \frac{2C\partial_0 r}{\pi} \left[\gamma \cos^{-1}\gamma - \sqrt{1-\gamma^2} \right] - \frac{2C b_0^2}{\pi}$$

$$- \frac{C \partial_0 r}{\pi} \left[\alpha \cos^{-1}\alpha - \sqrt{1-\alpha^2} + \delta \cos^{-1}\delta - \sqrt{1-\delta^2} \right]$$

(A-30)

where

$$\gamma = \frac{z_0}{r}$$

(A-31)

$$\alpha = \frac{z_0 - 2b_0}{r}$$

(A-32)

$$\delta = \frac{z_0 + 2b_0}{r}$$

(A-33)

BIBLIOGRAPHY

Ashe, J. B., Ph.D. dissertation, The University of Texas (1961) unpublished.

Berko, S. and Plaskett, J. S., Phys. Rev. 112, 1877 (1958).

Berko, S., Phys. Rev. 128, 2166 (1962).

Castillo-Bahena, R., Ph.D. dissertation, The University of Texas (1957) unpublished.

Castillo-Jimenez, F., Ph.D. dissertation, The University of Texas (1958) unpublished.

Deiterman, L., Jr., M.A. thesis, The University of Texas (1957) unpublished.

DeZafra, R. L., Physics Department Technical Report No. 101, University of Maryland, May 1958.

Dwight, H. B., Tables of Integrals and other Mathematical Data, (The Macmillan Company, New York, 1961).

Eckart, C., Phys. Rev. 51, 735 (1937).

Green, R. E. and Stewart, A. T., Phys. Rev. 98, 486 (1955).

Hall, J. D., Ph.D. dissertation, The University of Texas (1962) unpublished.

Heitler, W., Quantum Theory of Radiation (Oxford University Press, 1944).

Lang, L. G., "Angular Correlation of Annihilation Radiation from Solids," Carnegie Institute of Technology Report, Sept. 1956.

Lovseth, J., "Positronium Formation and Dynamics in Aluminum Oxide," Kjeller Research Establishment Report, Aug. 1962.

Millett, W. E. and Castillo-Bahena, R., Phys. Rev. 108, 257 (1957).

Siegbahn, K., Beta- and Gamma- Ray Spectroscopy (North-Holland Publishing Co., Amsterdam, 1955).

Stewart, A. T., Phys. Rev., 99, 594 (1955).

Trumpy, G., Phys. Rev. 118, 668 (1960).

VITA

Charles Joseph Vesely was born in Omaha, Nebraska, on June 20, 1939, the son of Charles Edward Vesely and Marguerite Marie Vesely. He was graduated from Wurtsmith Memorial High School, Clark Air Force Base, Luzon, Philippine Islands, in May, 1957 and entered The University of Southern California the following September. In September, 1958, he transferred to The University of Texas, where he received a Bachelor of Science degree in physics and a Bachelor of Arts degree in mathematics in January, 1962. During the summers of 1958 and 1959 he attended San Antonio Junior College. While in college he was a member of the A. F. R. O. T. C. and upon graduation he was commissioned a Second Lieutenant in the United States Air Force. Since then, he has been assigned to the graduate school of The University of Texas under the Air Force Institute of Technology Civilian Institutions Program.

Permanent Address: Box 603
Randolph A. F. B.
Texas

This thesis was typed by Martha Kaye Austin Vesely.